European Journal of Medicinal Chemistry 292 (2025) 117657

Contents lists available at ScienceDirect

European Journal of Medicinal Chemistry

journal homepage: www.elsevier.com/locate/ejmech

Research paper

Enhancing the activity of γ-hydroxy lactone derivatives as innovative peroxisome proliferator-activated receptor γ non-agonists inhibiting cyclin-dependent kinase 5-mediated phosphorylation

Giulia Cazzaniga [a,b], Davide Capelli [c], Roberta Montanari [c], Enrico Mario Alessandro Fassi [a], Giovanni Grazioso [a], Andrea Tresoldi [a], Francesca Rinaldi [d], Enrica Calleri [d], Ivan Bassanini [e], Sergio Romeo [a,e], Mariangela Garofalo [f], Matteo Mori [a,*], Fiorella Meneghetti [a], Stefania Villa [a]

[a] Department of Pharmaceutical Sciences, University of Milan, via L. Mangiagalli 25, 20133, Milano, Italy
[b] Department of Science and High Technology, University of Insubria, via Valleggio 9, 22100, Como, Italy
[c] Istituto di Cristallografia, Consiglio Nazionale delle Ricerche, Strada Provinciale 35d, n. 9-00010, Montelibretti, 34149, Rome, Italy
[d] Department of Drug Sciences, University of Pavia, via T. Taramelli 12, 27100, Pavia, Italy
[e] Istituto di Scienze e Tecnologie Chimiche "Giulio Natta", Consiglio Nazionale delle Ricerche, Via Mario Bianco 9, 20131, Milano, Italy
[f] Department of Pharmaceutical Sciences, University of Padova, via F. Marzolo 5, 35131, Padova, Italy

ARTICLE INFO

Keywords:
Insulin resistance
PPARγ non-agonists
CDK5
Enantiomeric resolution
SC-XRD
SBDD
Binding affinity
Ligand-protein complex

ABSTRACT

Insulin resistance (IR) is a pathological condition in which tissues exhibit a reduced response to normal or elevated levels of insulin. Type 2 diabetes mellitus (T2DM) and Metabolic Syndrome are the most prevalent disorders associated with IR. Most of the glitazones, traditional anti-diabetic drugs acting as Peroxisome Proliferator-Activated Receptor γ (PPARγ) agonists, have been withdrawn from the market. To mitigate the serious adverse effects associated with PPARγ agonism, a new opportunity is represented by the inhibitors of PPARγ phosphorylation by the Cyclin-Dependent Kinase 5 (CDK5). Their mechanism of action is mediated by the stabilization of the PPARγ β-sheet containing Ser245. Recently, we identified 4-(4-bromophenyl)-3-hydroxy-5-(3-hydroxyphenyl)furan-2(5*H*)-one (**I**) as a PPARγ non-agonist, capable of blocking the phosphorylation of the enzyme without direct effects on either CDK5 or PPARγ.

Here, we isolated the two enantiomers of **I**, unambiguously defined their absolute configuration through single crystal X-ray diffraction and demonstrated by Grating-Coupled Interferometry binding assays that both **(*S*)–I** and **(*R*)-I** exhibited comparable affinity for PPARγ. Then, a library of 12 analogs was designed through structure-based modifications, optimizing the interactions within the ligand-binding domain. GCI analysis identified derivative **11**, featuring an oxyacetic group in place of the initial hydroxyl function of the reference compound **I**, as the most promising candidate (K_D = 186 nM). The crystal structure of the PPARγ-LBD/**11** complex revealed a hydrogen bond interaction with Arg280, further stabilizing the binding conformation. These findings highlight the potential of γ-hydroxy lactone derivatives as PPARγ modulators and provide a foundation for future drug development targeting IR.

1. Introduction

Insulin resistance (IR) is a pathological condition characterized by attenuated tissue response to normal or elevated insulin production. Type 2 diabetes mellitus (T2DM) and Metabolic Syndrome are the most common clinical pathologies associated with IR. With the rising prevalence of TD2M and obesity worldwide, there is an urgent demand for more effective treatment options, especially considering that most Thiazolidinediones (TZDs), which are traditional anti-diabetic drugs acting as potent Peroxisome Proliferator-Activated Receptor γ (PPARγ) agonists, have been withdrawn from the market due to several adverse effects (weight gain, fluid retention, increased incidence of cardiovascular events, and bone fractures) [1–4]. Among this class, pioglitazone is the only anti-diabetic drug acting on IR that is still clinically available. PPARγ plays a critical role in the management of IR. It is a ligand-activated transcription factor involved in the regulation of many

* Corresponding author.
E-mail address: matteo.mori@unimi.it (M. Mori).

https://doi.org/10.1016/j.ejmech.2025.117657
Received 25 February 2025; Received in revised form 9 April 2025; Accepted 17 April 2025
Available online 18 April 2025

cellular functions and pathways, particularly those related to the regulation of fatty acid metabolism and glucose homeostasis [5]. It controls and promotes the expression of adipokines, including adiponectin. Notably, serum adiponectin levels are decreased in patients with obesity, insulin resistance, cardiovascular diseases, and hypertension compared to healthy subjects [6]. As full PPARγ agonists, TZDs promote the recruitment of coactivators and the assembly of a transcription-competent complex. They stabilize the H12 helix of the AF2 region, which in turn inhibits the binding of the co-repressor, maintaining the protein in its active form [7].

Over the years, efforts have shifted toward developing new compounds with strong therapeutic potential but fewer side effects. Strategies have included the development of PPARα/γ dual agonists or PPARα/γ/δ pan-agonists, which can coordinate improvements in carbohydrate and lipid metabolism, as well as selective PPARγ modulators (SPPARγMs). These modulators offer an improved therapeutic profile over full agonists by inducing different conformational changes in the receptor, leading to distinct transcriptional outcomes [8–13]. Moreover, PPARγ antagonists—such as bexarotene, 2-phenylamino pyrimidine, and *N*-biphenylmethylindole derivatives—have also demonstrated robust antidiabetic effects in rodent models, suggesting that they may provide a safe alternative for treating insulin resistance and T2DM [14–18].

In the last years, the modulation of post-translational modifications (PTMs) has emerged as a promising strategy for developing safer treatments for IR. By targeting PTMs, researchers aim to fine-tune the activity of key proteins involved in insulin signaling and glucose metabolism without triggering broader effects. In this context, a new opportunity is represented by molecules acting as inhibitors of PPARγ phosphorylation by the Cyclin-Dependent Kinase 5 (CDK5), whose activity is known to increase in inflammatory conditions, such as obesity.

In 2010, Choi and colleagues identified a strong correlation between high-fat diets *in vivo* and the phosphorylation of PPARγ at Ser273 (equivalent to Ser245 in PPARγ isoform 1) by CDK5 [8]. Building on this discovery, they introduced a new class of non-agonist antidiabetic compounds that improved insulin sensitivity without the typical side effects associated with PPARγ agonists. By 2014, the same researchers demonstrated that CDK5-mediated phosphorylation of PPARγ-Ser245 did not impact its adipogenic activity but instead disrupted the regulation of specific genes linked to obesity and diabetes [19]. By inhibiting this specific phosphorylation, it may be possible to restore the normal regulation of these target genes, thereby enhancing insulin sensitivity [8,9].

A notable example is the non-agonist PPARγ ligand SR1664, which emerged as a highly effective inhibitor of PPARγ phosphorylation while exhibiting strong antidiabetic properties. In contrast to TZDs and other PPARγ agonists, SR1664 did not cause fluid retention, weight gain *in vivo*, or impair osteoblast mineralization in cell culture [14,20].

Unlike full agonists, PPARγ non-agonists exhibit weak transactivation activity because they do not interact with the H12 helix of PPARγ. Instead, their mechanism of action involves the stabilization of the β-sheet containing Ser245. This stabilization prevents Ser245 from reaching the catalytic site of CDK5, thereby preventing its phosphorylation [7,21,22]. Consequently, non-agonists do not increase the expression of adipogenic genes and cannot stimulate adipocyte differentiation; rather, they primarily affect genes involved in glucose and insulin tolerance. As a result, non-agonists enhance insulin sensitivity without promoting adipogenesis [7,8,22,23].

To identify new non-agonist drugs, we previously screened an in-house library of synthetic γ-hydroxy lactone derivatives for their ability to prevent CDK5-mediated PPARγ phosphorylation by using Surface Plasmon Resonance (SPR) technology-based experiments [23]. These molecules were selected due to their structural similarity to **BLI** (Chart 1), a natural product isolated from the fungus *Aspergillus terreus*, which has been reported in the literature as both a PPARγ partial agonist and a CDK5 inhibitor [24]. Among the tested candidates, 4-(4-bromophenyl)-3-hydroxy-5-(3-hydroxyphenyl)furan-2(5*H*)-one (**I**, Chart 1) emerged as the most promising, with an encouraging K_D value of 3.75 μM. Biological assays demonstrated that **I** effectively inhibited CDK5-mediated phosphorylation of PPARγ *in vitro*, primarily by stabilizing PPARγ and exerting a weak inhibitory effect on CDK5. It did not exhibit agonist or antagonist activities on PPARγ, thereby validating its non-agonist profile. Moreover, crystallographic data of the PPARγ-**I** complex allowed to define the structural features required to achieve selective phosphorylation inhibition [23]. Given its synergistic therapeutic potential and synthetic feasibility, **I** was used as a starting point for the development of new γ-hydroxy lactone-based compounds as innovative candidates for the treatment of IR.

In this work, we successfully isolated the two enantiomers of our reference compound **I**, unambiguously defined their absolute configuration through single crystal X-ray diffraction (SC-XRD) and investigated their specific activity. Next, we conducted computational experiments to rationally design more efficient PPARγ non-agonists, starting from the crystal structure of the PPARγ/**I** complex (PDB ID 8ADF). This approach led to the discovery of optimized derivatives (Chart 1) with higher affinity for PPARγ. In addition, crystallographic studies were performed on the complex between PPARγ and the most promising analog to reveal its specific binding mode, thus providing a deeper understanding of the features necessary to enhance the affinity for the target. These findings not only validate the potential of modulating PTMs for improved insulin sensitivity but also pave the way for a new generation of selective PPARγ non-agonists that could revolutionize the treatment of insulin resistance. The integration of advanced computational design with detailed crystallographic analyses offers a solid foundation to future developments,

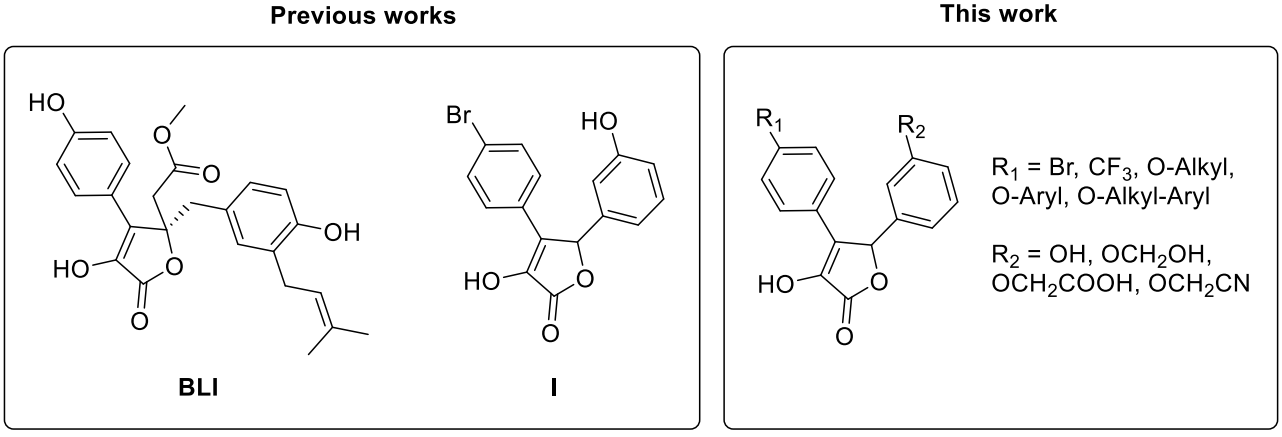

Chart 1. Chemical structures of **BLI**, reference compound **I**, and the new derivatives investigated in this work.

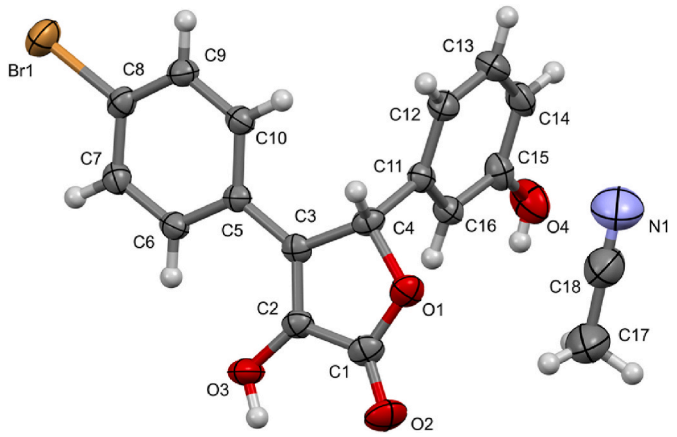

Fig. 1. Thermal ellipsoid diagram of the asymmetric unit of **(*S*)-I**, with the arbitrary atom-numbering scheme. Displacement ellipsoids are drawn at the 40% probability level.

which will represent a significant step forward, potentially leading to more precise and safer therapeutic interventions.

2. Results and discussion

2.1. Enantiomer-specific activity

2.1.1. Enantiomer separation

In our previous work, we identified compound **I** as a PPARγ non-agonist for the treatment of IR [23]. Given the presence of a chiral center and the potential for enantiomers to exhibit distinct biological activities, we developed a protocol for their separation. Therefore, **I** was synthesized following the literature procedure, leading to the racemic mixture [23]. Then, the separation of the two enantiomers (**I-E1** and **I-E2**) was performed via semi-preparative chiral RP-HPLC, affording high purity and excellent enantiomeric excess (98.83 % ee and 98.60 % purity for **I-E1**, 98.74 % ee and 97.89 % purity for **I-E2**).

2.1.2. Crystallographic analysis

Determining the absolute configuration of enantiomers is essential for understanding chiral discrimination mechanisms and predicting the enantioselective behavior of chiral drugs at the molecular level. Therefore, to establish the absolute configuration of the stereoisomers of **I**, we attempted their crystallization under various conditions. After several trials, we obtained small, but nicely diffracting crystals of **I-E1** by sublimating a water-acetonitrile solution of the compound. **I-E1** crystallized in the monoclinic system with space group $P2_1$, incorporating a molecule of acetonitrile in the asymmetric unit. The thermal ellipsoid diagram, indicating the arbitrary atom-numbering scheme used in the discussion, is reported in Fig. 1. The presence of the bromine atom as an anomalous scatterer allowed for the unambiguous determination of the absolute configuration of the chiral center as (*S*). In detail, the Flack parameter, calculated using the Parson's method, refined to −0.012(5), indicating high reliability in the determination [25]. Therefore, compound **I-E1** will henceforth be designated as **(*S*)–I**, while the other enantiomer (**I-E2**) will be referred to as **(*R*)-I**.

Table 1
H-bond geometry (D: Donor, A: Acceptor).

	D-H/Å	H … A/Å	D … A/Å	D-H … A/°
C6–H6···O3°	0.930(3)	2.316(3)	2.969(4)	126.9(2)
C9–H9···O4^{I}	0.930(3)	2.761(3)	3.448(4)	131.6(2)
O4–H4A···N1^{II}	0.75(6)	2.14(6)	2.877(6)	170(6)
O3–H3···O2^{III}	0.84(5)	1.88(6)	2.684(3)	158(6)

Equivalent positions: ^{0}x,y,z; ^{I}1-x,1/2+y,2-z; ^{II}x,y-1,z; ^{III}-x,y-1/2,1-z.

The γ-hydroxy lactone ring is flat and almost coplanar with the 4-bromophenyl substituent. The best mean planes of the two rings are inclined at 9.1°, and the torsional angle calculated for C4–C3–C5–C10 is −6.5(4)°. This arrangement is stabilized by an intramolecular H-bond between C6–H and O3. Conversely, the chiral center at C4 is in a classical tetrahedral geometry, with the 3-hydroxyphenyl group almost perpendicular to the best mean plane of the lactone (85.0°). In detail, the torsional angle calculated for C3–C4–C11–C12 is 123.0(3)°. An analysis performed using CSD Mogul confirmed that all structural parameters are within the expected limits for similar compounds [26,27]. The crystal packing is mainly ensured by H-bonds, established between the carbonyl oxygen and the hydroxyl group of the lactone rings, forming zipper-like chains along the *b* axis (Fig. 2). Additionally, the acetonitrile molecule interacts with the hydroxyl group of the phenol moiety through an H-bond. CπH … π and CπH … O contacts marginally contribute to the stabilization of the structure. A full account of the H-bonds is provided in Table 1.

The visualization of the intermolecular contacts was also aided by the analysis of the Hirshfeld surface (HS), mapped over the normalized contact distance (d_{norm}) [28]. The d_{norm} property (Fig. 3A) was visualized with a red-white-blue color scheme, based on the length of the intermolecular contacts with respect to the sum of the van der Waals radii. The analysis of the HS revealed the presence of three intense red spots, representing the short-range contacts between the lactone rings and between the phenol moiety and the acetonitrile molecule. The two-dimensional (2D) fingerprint of the HS (Fig. 3B), providing a visual summary of the contribution of each contact type and the relative area of the surface corresponding to it, confirmed the presence of these interactions, visualized as long spikes in the lower left part of the graph. C–H contacts occupied the wings of the plot, while the remaining portions indicated non-specific H–H interactions.

2.1.3. Affinity assay

Grating-Coupled Interferometry (GCI), representing an evolution of

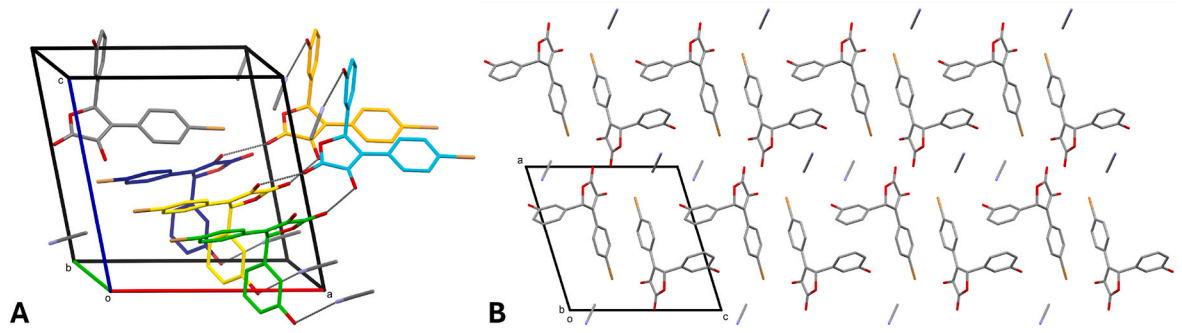

Fig. 2. A. Stick model of **(*S*)–I**, showing the main H-bonds, in an arbitrary view. Hydrogen atoms are omitted for clarity. **B.** Stick model of **(*S*)–I**, showing the packing along the *b* axis. Hydrogen atoms are omitted for clarity.

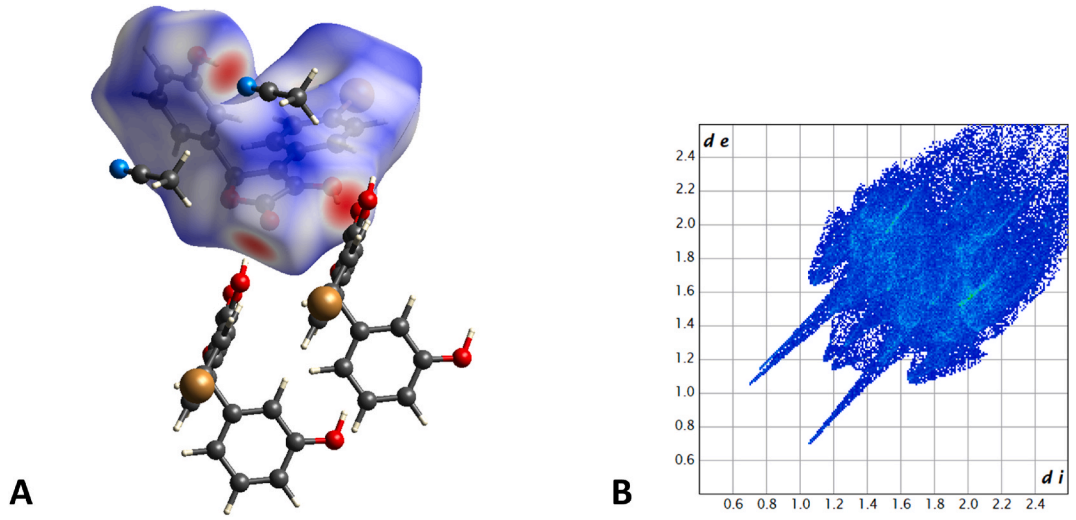

Fig. 3. A) HS mapped over d_{norm} with a fixed color scale in the range −0.6638 au (red) – 1.3201 au (blue), based on the length of the intermolecular contacts with respect to the sum of the van der Waals radii (red: shorter; blue: longer; white: same). **B)** 2D fingerprint plot of the HS of **(*S*)–I**. The graphical representation provides a summary of the frequency of each combination of d_e (distances from the HS to the nearest nucleus outside the surface) and d_i (distances from the HS to the nearest nucleus inside the surface) across the HS. Points with a lower contribution to the surface are colored blue, while green indicates larger contributions. (For interpretation of the references to color in this figure legend, the reader is referred to the Web version of this article.)

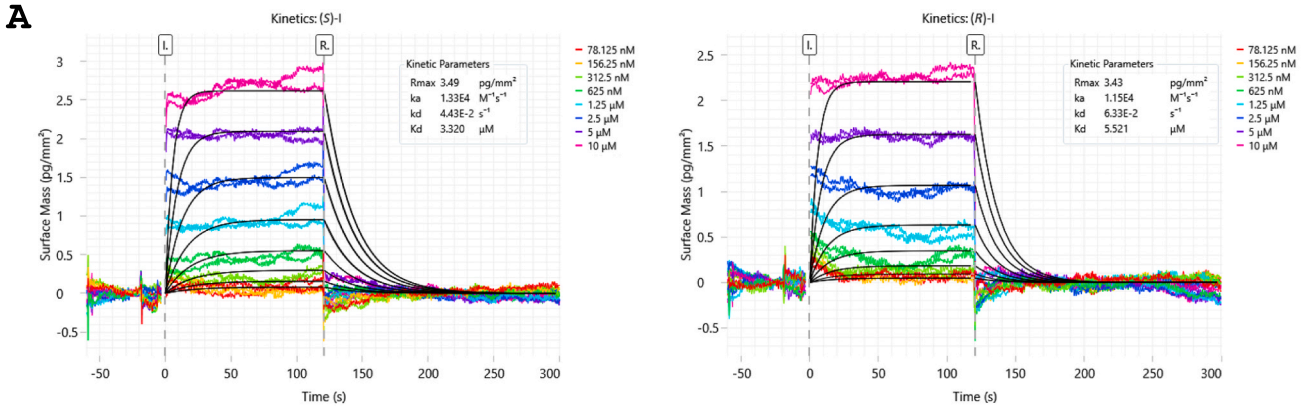

B

Ligand	k_a ($M^{-1}s^{-1}$)	k_d (s^{-1})	K_D (µM)
(*S*)-I	1.33 x 10^{-4}	4.43 x 10^{-2}	3.320
(*R*)-I	1.15 x 10^{-4}	6.33 x 10^{-2}	5.521

Fig. 4. A) Sensorgrams derived from the kinetic analyses of **(*S*)–I** and **(*R*)-I** in the interaction with PPARγ. **B)** Equilibrium dissociation constant (K_D) and rate constants (k_a and k_d) for the interaction between PPARγ and the two ligands.

Surface Plasmon Resonance (SPR) for the measurement of biomolecular interactions [29], was employed to determine the PPARγ binding affinity (K_D) to **(*S*)–I** and **(*R*)-I**, whose stability in the assay conditions had been previously verified. PPARγ was immobilized onto the sensor chip, and the two enantiomers were tested in the conditions described in the Materials and Methods section. **(*S*)–I** and **(*R*)-I** showed comparable K_D values (Fig. 4), indicating similar binding affinities for the two enantiomers of the reference compound **I**.

In light of these findings, and given the greater synthetic accessibility of the racemic form, **(*R*,*S*)–I** (henceforth referred to as **I**) was selected as a promising starting point for the development of novel γ-hydroxy lactone-based compounds, serving as innovative candidates for the treatment of IR.

2.2. *Cytotoxicity evaluation*

Compound **I** was subjected to cytotoxicity tests to evaluate the biosafety of the lactone scaffold. The viability assays confirmed that compound **I** did not affect the metabolic activity of the PNT2 human prostate cell line for concentrations up to 50 µM (Fig. S1). This favorable safety profile further supported the use of racemic compound **I** as a starting point for the development of innovative PPARγ non-agonists.

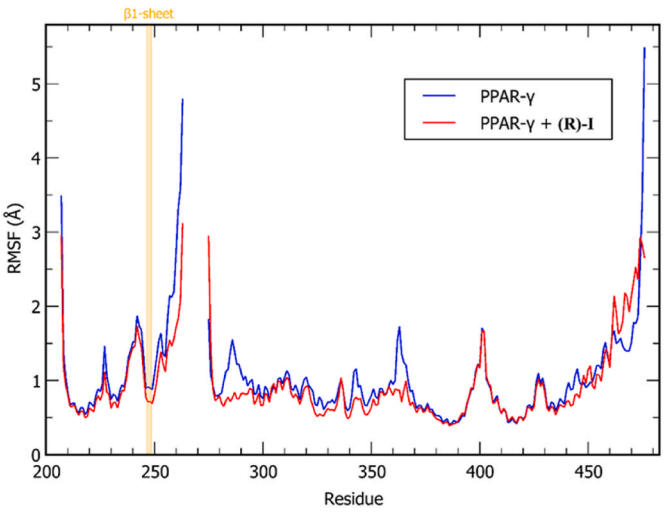

Fig. 5. RMSF plot of the backbone atoms of PPAR-γ (blue) compared to PPAR-γ complexed with compound (***R***)-**I** (red), considering the whole MD simulation time (2 × 250 ns). The β1-sheet portion is highlighted in orange. The gap in the plot indicates the missing loop (Lys263-Lys275) positioned upon the binding site. (For interpretation of the references to color in this figure legend, the reader is referred to the Web version of this article.)

2.3. Computational studies

2.3.1. Root Mean Square Fluctuation (RMSF) analysis

Despite the significant therapeutic potential of targeting CDK5-mediated phosphorylation, available data on this topic remain limited. Although the crystal structure of the PPARγ/CDK5/p25 complex has not been solved yet, several computational studies have explored the interaction mechanisms between these proteins. In our previous studies, we elucidated the mechanism by which CDK5 inhibits PPARγ phosphorylation. In-silico investigations indicated that for Ser245 to be properly accommodated in the CDK5 active site, an expansion of the loop containing this residue is required [21]. This process involves a temporary unfolding of the adjacent β1-sheet, a crucial step that facilitates the movement and proper exposure of the serine residue, thereby making it available for phosphorylation [21,30].

Interestingly, the crystal structure of the PPARγ/I complex (PDB ID 8ADF) revealed that compound **I** formed a direct hydrogen bond with Ser342. This interaction is particularly significant because it has been suggested as a potential inhibitory mechanism for CDK5-mediated phosphorylation of PPARγ at Ser245. By binding to Ser342, **I** may hinder the required unfolding of the β1-sheet, thereby preventing the proper accommodation of Ser245 within the CDK5 active site [21,23]. The ligand-induced reduction in the dynamics of the β-sheet impedes the phosphorylation process, offering a potential mechanism through which **I** could serve as an inhibitor of CDK5-mediated PPARγ phosphorylation. Therefore, we decided to further investigate our compound's potential to stabilize the β-sheet portion of PPARγ through Root Mean Square Fluctuation (RMSF) analysis, to evaluate whether the binding of **I** could induce the stabilization of the PPARγ structure. RMSF measures the average deviation of protein residues over time from a reference position, providing valuable information about which portions of the protein fluctuate from their mean structure [31]. We calculated the RMSF for the protein alone and in complex with **I** over the entire duration of the molecular dynamics (MD) simulation. Given that the compound was synthesized as a racemic mixture but only the (*R*) enantiomer was observed in the crystal structures, we selected **(*R*)-I** as a reference for the computational analysis. As shown in Fig. 5, the interaction of **(*R*)-I** reduces the overall flexibility of PPARγ and, most importantly, increases the stability of the β1-sheet portion of the protein, further confirming its hypothesized inhibitory mechanism.

Table 2
ΔG and K_D values for compounds **1–12**. Computational studies have been performed on (*R*)-enantiomers, whereas the GCI assays on the racemic compounds.

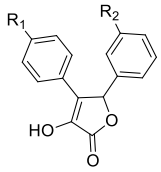

Code	R_1	R_2	Avg ΔG (kcal/mol)[a]	K_D (μM)
I	Br	OH	−25.5	3.80
1	CF_3	OH	−26.7	0.30
2	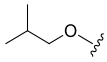	OH	−28.3	7.71
3	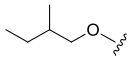	OH	−41.0	48.77
4	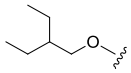	OH	−40.6	>50
5	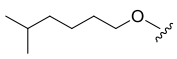	OH	−42.1	>50
6	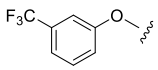	OH	−41.2	>50
7	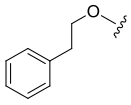	OH	−42.7	20.27
8	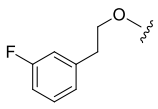	OH	−39.6	>50
9	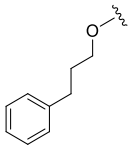	OH	−41.3	>50
10	Br		−29.8	4.08
11	Br	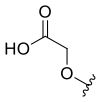	−39.4	0.19
12	Br		−35.7	0.79

[a] Data are from two replicates.

2.3.2. Generation of a new library

The X-ray crystal structure of the PPARγ/**I** complex (PDB ID 8ADF) [23] served as the starting model for computational studies aimed at generating a library of optimized derivatives. In detail, the Chain B/**(*R*)-I** complex (see Materials and Methods for details) was utilized to screen a collection of approximately 500 analogs, generated by

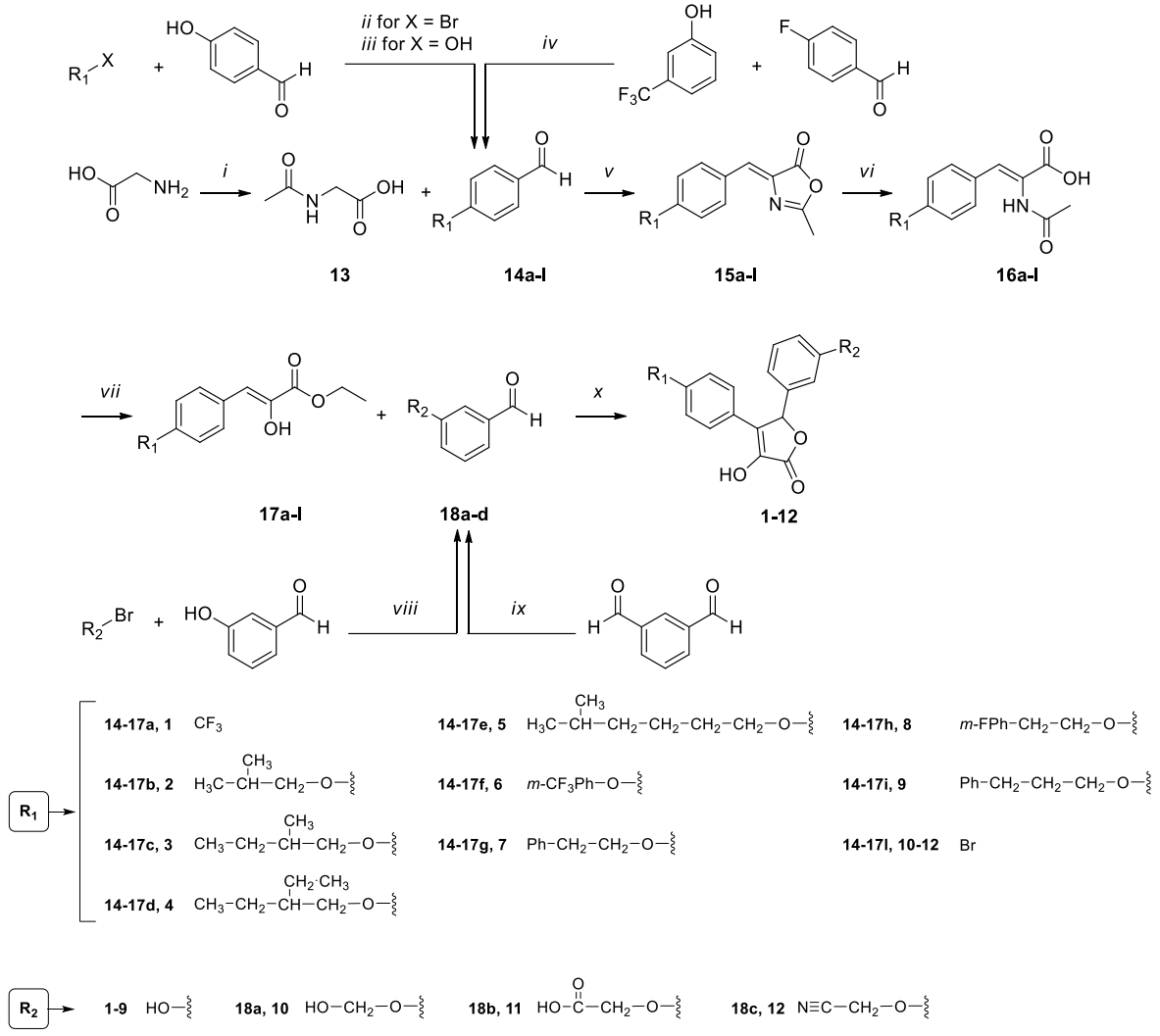

Scheme 1. *Reagents and conditions: i)* Ac_2O, vinegar, 20 min, RT; *ii)* K_2CO_3, dry MeCN, 5–48 h, reflux, N_2 atm.; *iii*) DIAD, PPh_3, dry THF, overnight, RT, N_2 atm.; *iv)* K_2CO_3, dry DMSO, 10 min, 140 °C, N_2 atm., MW; *v)* NaOAc, Ac_2O, 5–12 h, 100 °C; *vi)* vinegar, 3 h, reflux; *vii*) conc. HCl, EtOH, 5 h, reflux; *viii*) K_2CO_3, dry MeCN, 4–12 h, reflux, N_2 atm.; *ix)* $NaBH_4$, dry THF, dry EtOH, 1 h, 0 °C, N_2 atm.; *x)* DBU, dry DMF, 4 h, 0 °C, N_2 atm.

modifying two features of the ligand. In series A, the bromine atom was replaced with various substituted –OR groups to more effectively occupy the hydrophobic pocket within the active site. In series B, the hydroxyl group of the phenol ring was replaced with other moieties capable of enhancing the interaction with Arg280.

The whole library was subjected to docking calculations, and the top 30 analogs, ranked based on their docking score, were selected for further analysis through two independent 250 ns MD simulations (see Materials and Methods for details). From MM-GBSA analyses performed on **(*R*)-I**, we obtained ΔG values of −24.4 ± 0.1 kcal/mol and −26.6 ± 0.2 kcal/mol for replicas 1 and 2, respectively. The average binding free energy (ΔG = −25.5 kcal/mol) served as a reference to identify analogs with improved theoretical binding affinity for the target. Among all the screened compounds, nine derivatives from series A (compounds **1–9**) and three from series B (compounds **10–12**) were selected to be synthesized based on their ΔG values and synthetic feasibility (Table 2).

2.4. Chemistry

All the compounds (**1**–**12**) were synthesized following previously established synthetic procedures (Scheme 1) [23], with subsequent optimization to align with green chemistry principles. The *N*-acetylation of glycine, which represents the first step in the production of all analogs, was carried out with an innovative, eco-friendly approach, recently developed in our laboratory. In detail, traditional organic solvents were replaced with bio-based alternatives derived from biowaste or inexpensive and easily accessible natural sources [32], resulting in a versatile and time-efficient procedure, minimal purification efforts, and good yields.

The so-obtained *N*-acetylated glycine (**13**) was then subjected to a cyclization reaction with a previously synthesized benzaldehyde derivative (series **14**) to afford products **15a-l**. Intermediates **14b,c,e,g-i** were obtained through a nucleophilic substitution between 4-hydroxybenzaldehyde and the appropriate bromo derivative. Intermediate **14f** was obtained by reacting 4-fluorobenzaldehyde and 3-(trifluoromethyl) phenol in a microwave-assisted nucleophilic aromatic substitution, while intermediate **14d** was accessed through a Mitsunobu reaction involving 2-ethyl-1-butanol and 4-hydroxybenzaldehyde.

Encouraged by the successful results achieved in the first step with vinegar as a substitute for the traditional solvent, we opted to extend the use of this bio-based alternative to other synthetic steps requiring acidic conditions. Compounds **15a-l** were hydrolyzed in vinegar leading to the amide intermediates **16a-l**. Then, a one-pot reaction led to the hydrolysis of the acetoamide moiety and the esterification of the pyruvic acid residue, using concentrated HCl and EtOH. The resulting esters (**17a-l**) were cyclized with commercially available (intermediate **18a**) or

A

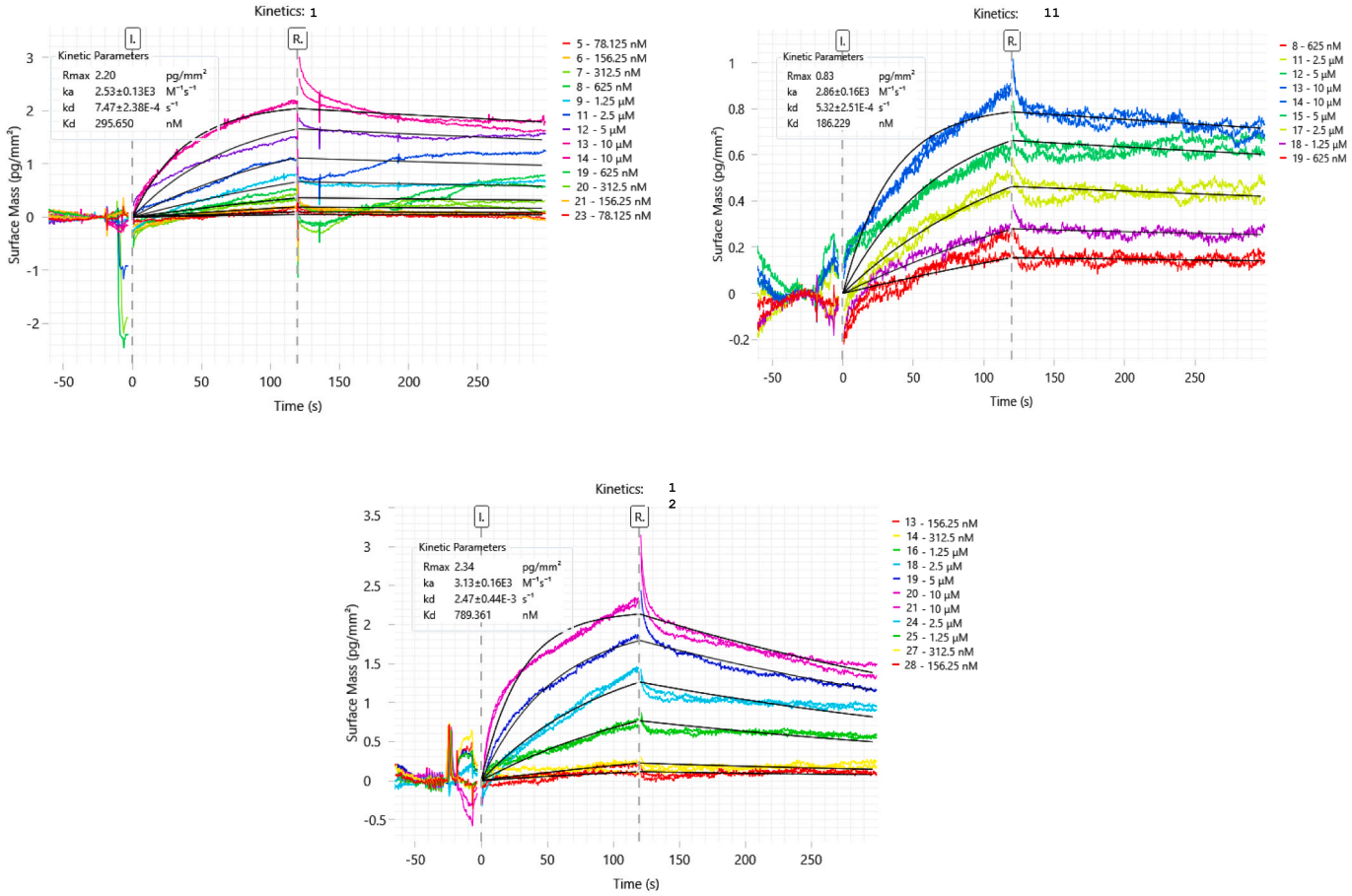

B

Ligand	k_a ($M^{-1}s^{-1}$)	k_d (s^{-1})	K_D (nM)
1	2.53 x 10^{-3}	7.47 x 10^{-4}	295
11	2.86 x 10^{-3}	5.32 x 10^{-4}	186
12	3.13 x 10^{-3}	2.47 x 10^{-3}	789

Fig. 6. A) Sensorgrams derived from the kinetic analyses of **1** (top left), **11** (top right), and **12** (bottom) in the interaction with PPARγ. **B)** Equilibrium dissociation constant (K_D) and rate constants (k_a and k_d) for the interaction between PPARγ and the three ligands.

previously synthesized (intermediate **18b-d**) benzaldehyde derivatives, to obtain the final γ-hydroxy lactone-based compounds **1–12**. In detail, intermediate **18b** was obtained by a selective reduction of one of the aldehyde groups of isophthalaldehyde using $NaBH_4$, whereas **18c, d** were synthesized by a nucleophilic substitution between the appropriate bromo derivative and 3-hydroxybenzaldehyde.

2.5. Evaluation of PPARγ affinity

GCI was employed to measure the binding affinity (K_D) of **1**–**12** to PPARγ. The receptor was immobilized onto the sensor chip, and **1–12** were tested in the conditions described in the Materials and Methods section. The resulting K_D values are shown in Table 2.

Among the members of series A, where the bromine atom was substituted with bulkier aliphatic or aromatic moieties, only compound **1**, featuring the slightly larger CF_3 group, exhibited enhanced affinity for the target (**1** K_D = 295 nM *versus* **I** K_D = 3.75 μM) (Fig. 6). Compound **2**, functionalized with the smallest aliphatic chain in the series, retained sufficient interaction with the target (K_D = 7.71 μM). Conversely, larger substituents (**3**–**9**) likely hindered the compounds' ability to access and properly fit within the binding cavity. This effect could be attributed to steric clashes caused by the long, highly flexible loop (Lys263–Lys275) that spans across the binding site, a region that remains unresolved in X-ray crystallographic analyses. Consequently, the ΔG values calculated for compounds **3**–**9** should be considered as artifacts, as the docking simulations place the ligands in the designated pocket based solely on steric compatibility, without accounting for whether the ligands can effectively access the pocket.

Series B was designed to improve the interactions with Arg280, a key residue within the active site. Compound **10** showed a comparable K_D value to the parent compound, while derivatives **11** and **12** showed more than a tenfold improvement in affinity (**11** K_D = 186 nM, **12** K_D = 789 nM) (Fig. 6). In this case, computational studies accurately predicted the ΔG values of the compounds. Specifically, both compounds

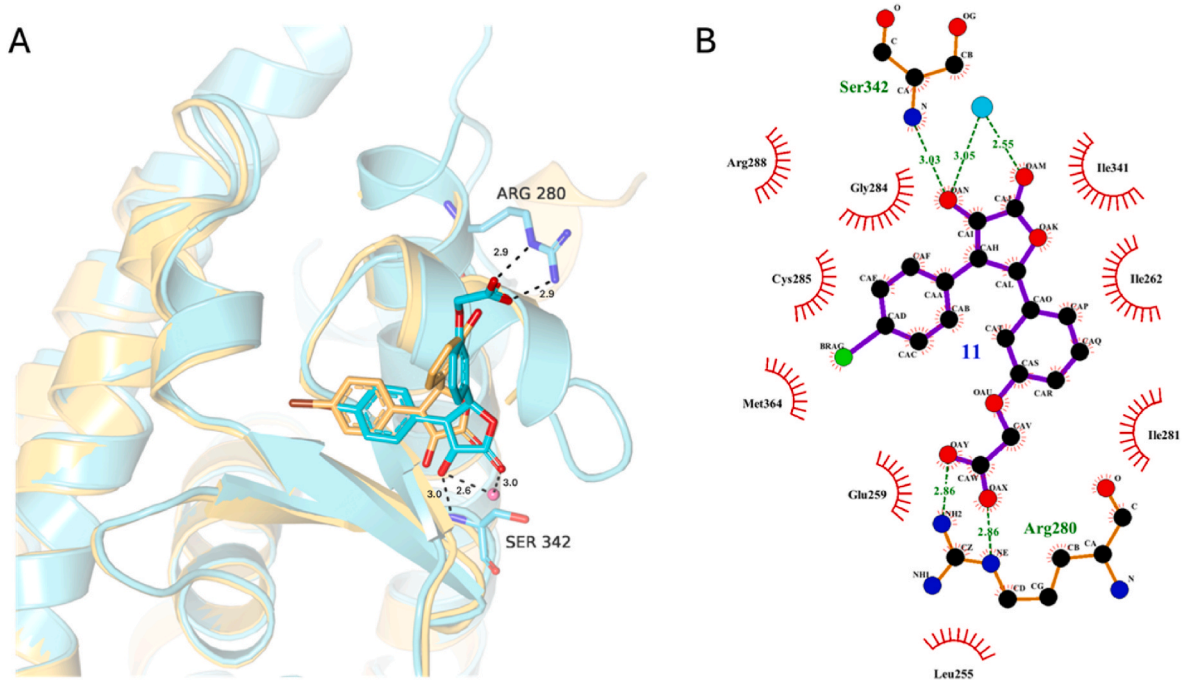

Fig. 7. A) Superposition between **I** (orange; PDB ID 8ADF) and **11** (cyan; PDB ID 9HX2) within PPARγ-LBD generated with The Protein Imager [34], showing the interactions of **11** with the residues of the protein (light cyan sticks). Hydrogen bonds are depicted as black dashes and the water molecule as a pink sphere. **B)** 2D Representation of the ligand interactions generated with Ligplot^{+} [35], showing hydrogen bonds (green dashes) and hydrophobic contacts (red spline curves). The water molecule is depicted as a cyan sphere. (For interpretation of the references to color in this figure legend, the reader is referred to the Web version of this article.)

11 and **12** exhibited lower ΔG values (−39.4 and −35.7 kcal/mol, respectively) compared to the reference molecule **I** (−25.5 kcal/mol). Conversely, for compound **10**, we obtained a ΔG value only slightly more negative (−29.8 kcal/mol), well correlating with the slight improvement in the experimental dissociation constant ($K_D = 4.10$ μM). The substitution with a carboxylic (**11**) or nitrile group (**12**), combined with the flexibility of Arg280, likely facilitated the formation of new hydrogen bond interactions with the side chain of the residue, thus contributing to the marked increase in binding affinity. Therefore, this second approach proved to be highly successful, leading to the identification of the most potent candidate (**11**) across both series. The modifications not only significantly enhanced the binding affinity but also demonstrated the effectiveness of strategic substitutions in optimizing interactions with the target, demonstrating their potential to enhance the overall potency of the compounds. Most notably, **11** showed stronger binding affinity for PPARγ than the previously reported PPARγ non-agonists SR1664, UHC1, and AM-879 [19,33]. These literature compounds have also demonstrated promising *in vivo* efficacy, further supporting the potential of our candidate for future therapeutic development [19,33].

2.6. Binding of 11 to PPARγ-LBD

To gain detailed structural insights into the binding mode of the most potent compound, the crystal structure of the PPARγ-LBD/**11** complex was determined at a resolution of 2.85 Å using diffraction data collected from apo-crystals soaked with the ligand. The electron density clearly reveals the (*R*) enantiomer within molecule A of the crystallographic dimer, with the ligand occupying the same binding site as the parent compound **I**, located between helix 3 (H3) and the β-sheet (Fig. 7A). The ligand retains the ability to form a hydrogen bond with Ser342 of the β-sheet, a key feature that may prevent the phosphorylation of Ser245 by CDK5. Compared to **I**, compound **11** is slightly shifted and effectively interacts with Arg280 of helix 3 through its extended carboxylic group, as initially hypothesized during the design of series B compounds. As shown in Fig. 7B, the oxygen atoms of the carboxylic group are positioned at a hydrogen-bonding distance of 2.9 Å from the nitrogen atoms of the flexible side chain of Arg280, ensuring a highly efficient interaction. In addition, the short distance between the oxygen atom located at the *meta* position of the ligand's benzene ring and the carbonyl oxygen of Arg280 suggests the presence of a strong dipole-dipole interaction,

Table 3
Crystal data and structural refinement statistics for **I-E1**.

Compound	I-E1	
Empirical formula	$C_{18}H_{14}BrNO_4$	
Formula weight	388.21	
Temperature	293(2) K	
Wavelength	0.71073 Å	
Crystal system	Monoclinic	
Space group	$P2_1$	
Unit cell dimensions	$a = 12.4484(3)$ Å	$\alpha = 90°$
	$b = 5.71790(10)$ Å	$\beta = 107.061(3)°$
	$c = 12.5919(4)$ Å	$\gamma = 90°$
Volume	856.83(4) Å^3	
Z	2	
Density (calculated)	1.505 Mg/m^3	
Absorption coefficient	2.419 mm^{-1}	
F(000)	392	
Crystal size	0.25 × 0.15 × 0.08 mm^3	
θ range for data collection	1.692–26.371°	
Index ranges	$-15 \le h \le 15$, $-7 \le k \le 7$, $-15 \le l \le 15$	
Reflections collected	17731	
Independent reflections	3503 [$R_{int} = 0.0265$]	
Completeness to $\theta = 25.242°$	100.0 %	
Refinement method	Full-matrix least-squares on F^2	
Data/restraints/parameters	3503/1/226	
Goodness-of-fit on F^2	1.052	
Final R indices [$I > 2\sigma(I)$]	R1 = 0.0280, w$R2$ = 0.0621	
R indices (all data)	R1 = 0.0337, w$R2$ = 0.0639	
Absolute structure parameter	−0.012(5)	
Largest diff. peak and hole	0.420 and −0.301 e·Å^{-3}	
CCDC accession number	2400627	

Table 4
Summary of crystallographic analysis for crystals of the PPARγ-LBD/**11** complex.[a] Values in parentheses refer to the outer shell.

	PPARγ-LBD/11
Data collection	
Space group	*C2*
Cell dimension *a*, *b*, *c* [Å]	93.196, 61.182, 118.200
Wavelength [Å]	0.968
Resolution range [Å]	50.78–2.85
Last shell [Å]	2.90–2.85
R_{merge}	0.17 (1.16) [a]
Unique reflections	15066
Mean $(I)/\sigma(I)$	3.5 (1.0) [a]
Completeness	97.4 (99.7) [a]
No. of molecules in asymmetric unit	2
Refinement	
Resolution range [Å]	50.78–2.85
R_{work} [%]	22.3
R_{free} [%]	28.6
Bond lengths r.m.s.d. [Å]	0.003
Bond angles r.m.s.d. [deg]	0.643
PDB ID	9HX2

which further contributes to the stabilization of the binding. The positioning of the ligand is further stabilized by coordination with a water molecule, as well as multiple hydrophobic interactions with residues Leu255, Glu259, Ile262, Ile281, Gly284, Cys285, Arg288, Ile341 and Met364. These interactions collectively enhance the binding affinity, ensuring that the ligand remains firmly anchored within the binding site through both polar and non-polar forces. Compared to the parent compound **I**, the lower binding affinity constant observed for the derivative compound **11** in the GCI assay likely reflects the more complex and enhanced interaction network formed within the PPARγ-LBD.

3. Conclusion

In this study, we identified and optimized γ-hydroxy lactone derivatives as innovative PPARγ non-agonists capable of inhibiting CDK5-mediated phosphorylation. Starting from compound **I**, which demonstrated promising inhibition of PPARγ phosphorylation with minimal off-target activity, we refined its structure using both computational and crystallographic approaches. Enantiomeric separation and crystallographic analysis revealed that both enantiomers of compound **I** exhibited comparable binding affinities for PPARγ (3.320 μM and 5.521 μM for **(*S*)–I** and **(*R*)-I**, respectively). This equivalence in activity enables the practical use of these compounds as racemates, simplifying their synthesis and reducing production costs without compromising their efficacy. The use of racemic compound **I** as a starting point for the development of innovative PPARγ non-agonists was further supported by its favorable safety profile, as confirmed by cytotoxicity assays on PNT2 cells. Thus, we conducted computational studies to develop a new library of γ-hydroxy lactone derivatives with improved predicted binding affinities (-46.7 kcal/mol $< \Delta G < -26.7$ kcal/mol), culminating in compounds **11** and **12**, which demonstrated nanomolar K_D values (186 nM and 789 nM for **11** and **12**, respectively) and significantly enhanced interactions with critical residues in the PPARγ-LBD. These results were confirmed by crystallographic analyses, providing structural insights into their mechanism of action. A comparison of the PPARγ-LBD/**11** complex with PPARγ-LBD/**I** (PDB ID 8ADF) revealed a conservation of the key interaction with Ser342 and an enhanced binding to the side chain of Arg280, facilitated by the oxyacetic substituent.

Overall, our work represents a significant step forward in the development of safe and effective treatments for insulin resistance and related metabolic disorders. By targeting the post-translational regulation of PPARγ, these compounds offer a novel therapeutic strategy that could address the limitations of current treatments and pave the way for the development of next-generation antidiabetic drugs.

4. Materials and Methods

4.1. Enantiomeric separation

The separation of the enantiomeric mixture of compound **I** was performed by preparative HPLC on a Waters system using a Phenomenex Lux Cellulose-1 column 250 × 10 mm. Mobile phase: H_2O/MeCN 60:40 + 0.1 % TFA to H_2O/MeCN 0:100 + 0.1 % TFA in 15 min. Flow rate: 5 mL/min. Wavelength: 254 nm. Temperature: 25 °C. The separation procedure yielded the first enantiomer (tR = 8.07 min) at 98.83 % ee and 98.60 % purity, and the second enantiomer (tR = 9.18 min) at 98.74 % ee and 97.89 % purity. The so-obtained stereoisomers were subjected to crystallographic analysis and biological evaluations. The optical rotatory powers are as follows: $[\alpha]_D = +6.1508 \pm 0.0507$ (c = 2.3 mg/mL; solvent: MeOH; T = 26 °C) for **I-E1**, and $[\alpha]D = -3.7917 \pm 0.0225$ (c = 2 mg/mL; solvent: MeOH; T = 24 °C) for **I-E2**.

4.2. Determination of the enantiomeric configuration

X-ray diffraction-quality crystals of **I-E1** were obtained as colorless prisms from the sublimation of a 6:4 MeCN/H_2O solution. Intensity data were collected at 293(2) K with a Rigaku XtaLAB Synergy diffractometer (Rigaku, Tokyo, Japan), equipped with a microfocus PhotonJet Mo-Kα source and a HyPix-6000HE detector. Data collection was performed with omega scans with a step size of 0.5° and an exposure time of 43 s/frame. A total number of 17,731 Bragg reflections (with a high degree of redundancy) were collected, giving a metrically monoclinic unit. The analysis of the systematic absences indicated the space group $P2_1$. Intensity data were integrated and corrected for Lorentz-polarization effect, using the Rigaku CrysAlisPRO 1.171.42.90a software (CrysAlisPro Software System, Rigaku Oxford Diffraction/Agilent Technologies UK Ltd, Yarnton, UK). The same program was employed to perform a multi-scan empirical absorption correction of the diffraction data. The structure was solved by direct methods using SIR2019/3 [36] and completed by iterative cycles of full-matrix least squares refinement on F_o^2 and ΔF synthesis using SHELXL-2019/3 [37] within the WinGX suite (WinGX v.2023.1 [38]). Hydrogen atoms were introduced at calculated positions in their described geometries and allowed to ride on the attached atom with fixed isotropic thermal parameters (1.2 U_{eq} of the parent atom for aromatic and methine groups; 1.5 U_{eq} for methyl groups). Oxygen-bound atoms were located in the Fourier map and refined isotropically. The structure was analyzed by PARST [39] (H-bond geometry), Mogul [26,27] (comparison with CCDC-deposited structures), Mercury 2023.3.0 [40] (geometrical features, crystal packing, and intermolecular interactions), and CrystalExplorer21 [41] (HS analysis). Graphical representations were rendered with Mercury and CrystalExplorer21, starting from the CIF file compiled by WinGX. All relevant crystallographic information is reported in Table 3 (see CIF file for further details).

4.3. Cytotoxicity assay

The PNT2 (European Collection of Authenticated Cell Cultures, ECACC, UK) human prostate cell line was purchased from Sigma-Aldrich. The cells were cultured at 37 °C and 5 % CO_2 in RPMI 1640 (Gibco Laboratories), supplemented with 10 % FBS (Gibco Laboratories), 1 % of 100 U/mL penicillin/streptomycin (Gibco Laboratories), and 2 % L glutamine (Gibco Laboratories). The cells were seeded at a density of 1×10^4 cells/well in 96-well plates and maintained under standard growth conditions. After 24 h, cells were treated with compound **I** in the range of 0.5–50 μM to a final volume of 100 μL. After 96 h, cell viability was assessed by MTS assay, according to the manufacturer's protocol (Cell Titer 96 Aqueous One Solution Cell Proliferation Assay; Promega, Nacka, Sweden) using a 96-well-plate spectrophotometer (Varioskan Flash Multimode Reader; ThermoFisher Scientific, Waltham, MA, USA) set at λ = 490 nm. The absorbance value of

untreated cells was set at 100 % (control), and the viability of treated cells was expressed as a percentage of the control. Three independent experiments were performed for each condition.

4.4. Computational studies

4.4.1. Model selection and preparation

The X-ray crystal structure of the PPARγ/**I** complex (PDB ID 8ADF) was used as the starting point to perform computational studies [23]. The model consists of a PPARγ dimer (*i.e.*, Chain A and B), each complexed with an **(*R*)-I** molecule. Notably, each ligand interacts with a different binding mode with the active site. After a careful visual inspection of the different binding modes assumed by **(*R*)-I**, only Chain B was selected for the computational analysis. The missing loops (Thr238-Ser245, Gly258-Ala278, and Leu453-Leu468) were fully or partially reconstructed by applying the computational homology modeling technique. In detail, the first and last loops were fully built using Chain A as a template model, while the second loop was partially built using the PPARγ structure available in the Protein Data Bank (PDB ID 6L89), in which the protein is complexed with Butyrolactone 1 (**BLI**) [24]. However, only the Glu259-Lys263 and Lys275-Val277 segments could be added to Chain B. Finally, the crystallization water (residue #640 of the crystal structure) was maintained due to the important coordination role with the OH group of the lactone (water bridge with Ser342). The resulting model was then optimized and minimized using the Protein Preparation Wizard tool of Maestro software (Schrödinger, LLC, New York, NY, USA), which allowed us to: (I) complete the complex structure by adding the missing hydrogens and creating the disulfide bonds; (II) check the protonation state of the residues at pH 7.0; (III) remove the atomic clashes; and (IV) assign the OPLS4 force field to the atoms.

4.4.2. Docking procedures

The new library was prepared using the "Reaction-Based Enumeration" tool available in the Maestro suite, adding simple, commercially available R groups and obtaining a total of about 500 mutated compounds. The docking grid was centered on the ligand, placed in the active site of the crystal structure of PPARγ (Chain B). Then, the docking protocol was validated through re-docking of compound **(*R*)-I**. Finally, the whole library was subjected to docking calculations, performed using Glide software implemented in Maestro, applying the extra-precision (XP) mode, to achieve the most favorable binding mode of the compounds within the active site [42]. The best docking pose by docking score exhibited by the best 30 ligands was selected for the subsequent MD simulations.

4.4.3. MD simulations

Before performing the MD simulations, the system was properly prepared. First, the protein was solvated in a TIP3P water box [43], whose edges were required to have a minimum distance of 10 Å from the protein surface. Then, a proper number of counter-ions was added to achieve charge neutrality (5 Na^+ atoms). To remove initial atom-atom clashes in the protein structure, the system was relaxed using a multi-step minimization protocol. Finally, in the equilibration phase, the system was heated to 300 K in 300 ps, and pressure was increased to 1 atm. During MD simulations, temperature and pressure were kept constant using Langevin thermostat [44] and Monte Carlo barostat [45], respectively. Production trajectories were run for 250 ns in two independent replicas (total 0.5 μs). AMBER22 was used to perform MD simulations. Molecular Mechanics-Generalized Born Surface Area (MM-GBSA) calculations [46] were performed to compute the ligand binding free-energy (ΔG) values considering the 500 MD frames (corresponding to 100 ns of simulation time) in which the ligand displayed the highest stability in the enzyme (the RMSD/time plot of the Cα atoms was considered). In these calculations, the single trajectory approach was applied, and the entropy contributions to the binding free energy were neglected.

4.4.4. RMSF calculation

The RMSF for the systems containing only the protein and the PPARγ/**(*R*)-I** complex were calculated considering the whole MD simulation time. In both cases, the initial crystal structure was used as a reference, and only the backbone atoms were included in the calculation. The calculation was performed using the "*gmx rmsf*" algorithm, available in the GROMACS software package (version 2018.8). XMGRACE (http://plasma gate.weizmann.ac.il/Grace) software was used to plot the results.

4.5. Chemistry

All starting materials, chemicals, and solvents were purchased from commercial suppliers (Sigma-Aldrich/Merck KGaA, Darmstadt, Germany; FluoroChem, Hadfield, UK; CarloErba, Cornaredo, Italy) and used as received. Anhydrous solvents were utilized without further drying. Aluminum-backed Silica Gel 60 plates (0.2 mm; Merck, Darmstadt, Germany) were used for thin-layer chromatography (TLC) to follow the course of the reactions. Silica gel 60 (40–63 μm; Merck) was used for the purification of intermediates and final compounds through flash column chromatography. Melting points were determined in open capillary tubes with a Stuart SMP30 Mp Apparatus (ColeParmer Stuart, Stone, UK). Optical rotatory powers were measured with a Jasco P-1010 polarimeter (Jasco, Easton, 85 MD, USA), using a microcuvette (l = 0.1 dm). ^{1}H NMR, ^{13}C NMR, and ^{19}F NMR spectra were acquired at ambient temperature with a Varian Oxford 300 MHz instrument (Varian, Palo Alto, CA, USA), operating at 300 MHz for ^{1}H, 75 MHz for ^{13}C, and 282 MHz for ^{19}F. ATR-FT-IR spectra were acquired with a Jasco FT/IR-610 (Jasco, Tokyo, Japan), equipped with an ATR sampling accessory. High-resolution mass spectra (HRMS) were acquired on a ThermoFisher Scientific Orbitrap Exploris 120 (ThermoFisher Scientific, Waltham, MA, USA) equipped with UHPLC and C18 column. The purity of the tested compounds (≥95 %) was assessed by reversed-phase HPLC on a Waters system (Waters, Milford, MA, USA), using a Grace VisionHT™ C18 Classic 5 μM, 250 mm × 4.6 mm column (Grace Davison Discovery Sciences, Deerfield, IL, USA) in the following operative conditions: mobile phase: 40:60H_2O/MeCN + 0.1 % TFA (isocratic mode); flow rate: 1 mL/min; detector λ: 254 nm; time: 20 min; temperature: 23 °C. All relevant spectra, chromatograms, and atom numbering used in NMR signal assignments are detailed in the Supplementary Materials.

Compounds **14a**, **14l**, and **18a** were purchased from commercial suppliers (Sigma-Aldrich/Merck KGaA, Darmstadt, Germany; FluoroChem, Hadfield, UK)

4.5.1. N-acetyl glycine (*13*)

Acetic anhydride (9.31 mmol, 3.5 eq.) was added to a solution of glycine (2.66 mmol, 1 eq.) in vinegar (1 mL), and the mixture was stirred for 20 min at room temperature. Then, the resulting precipitate was collected by filtration to afford the desired pure product as a white solid, without the need for further purification. Yield: 70 %. R_f: 0.60 (DCM/MeOH 8:2). Mp: 206–207 °C. ^{1}H NMR (300 MHz, DMSO-d_6) δ (ppm) 8.14 (s, 1H, H_5), 3.70 (d, J = 5.9 Hz, 2H, H_1), 1.82 (s, 3H, H_7).

4.5.2. 4-Isobutoxybenzaldehyde (*14b*)

General procedure A. The appropriate bromo derivative (1.96 mmol, 1.2 eq) was added at room temperature to a stirred solution of 4-hydroxybenzaldehyde (0.98 mmol, 1 eq.) and oven-dried K_2CO_3 (3.28 mmol, 4 eq.) in MeCN dry (3 mL). The mixture was stirred at reflux under a nitrogen atmosphere for 4–48 h depending on the starting compounds. The reaction mixture was extracted with EtOAc (3 × 5 mL), and the organic phase was dried over anhydrous Na_2SO_4, filtered, and evaporated *in vacuo*. The resulting solid was purified by flash column chromatography (cyclohexane/EtOAc 8:2). Reaction time: 48 h. Aspect: yellow oil. Starting reagent: 1-bromo-2-methylpropane. Yield: 80 %. R_f:

0.59 (cyclohexane/EtOAc 8:2). ^{1}H NMR (300 MHz, $CDCl_3$) δ (ppm) 9.87 (s, 1H, H_8), 7.82 (d, J = 8.8 Hz, 2H, H_4, H_6), 6.99 (d, J = 8.8 Hz, 2H, H_1, H_3), 3.80 (d, J = 6.5 Hz, 2H, H_{11}), 2.11 (hept, J = 6.7 Hz, 1H, H_{12}), 1.04 (d, J = 6.7 Hz, 6H, H_{13}, H_{14}).

4.5.3. 4-(2-Methylbutoxy)benzaldehyde (14c)

The compound was obtained according to General Procedure A. Purification: flash column chromatography (cyclohexane/EtOAc 95:5). Reaction time: 24 h. Aspect: colorless oil. Starting reagent: 1-bromo-2-methylbutane. Yield: 60 %. R_f: 0.68 (cyclohexane/EtOAc 9:1). ^{1}H NMR (300 MHz, $CDCl_3$) δ (ppm) 9.88 (s, 1H, H_8), 7.82 (d, J = 8.6 Hz, 2H, H_4, H_6), 6.99 (d, J = 8.6 Hz, 2H, H_1, H_3), 3.93–3.79 (m, 2H, H_{11}), 1.99–1.80 (m, 1H, H_{12}), 1.62–1.51 (m, 1H, $H_{13'}$, partially overlapped with H_2O), 1.34–1.23 (m, 1H, $H_{13''}$), 1.03 (d, J = 6.7 Hz, 3H, H_{14}), 0.96 (t, J = 7.4 Hz, 3H, H_{15}).

4.5.4. 4-(2-Ethylbutoxy)benzaldehyde (14d)

Diisopropyl azodicarboxylate (1.58 mmol, 1.08 eq.) was added dropwise at 0 °C to a solution of 4-hydroxybenzaldehyde (1.47 mmol, 1 eq.), 2-ethylbutan-1-ol (1.47 mmol, 1 eq.), and triphenylphosphine (1.58 mmol, 1.08 eq.) in dry THF (4.7 mL). The mixture was stirred at room temperature overnight, under a nitrogen atmosphere. The reaction mixture was evaporated *in vacuo*, and the crude residue was purified by flash column chromatography (cyclohexane/EtOAc 95:5) to afford the desired product as a yellow oil. Yield: 80 %. R_f: 0.39 (cyclohexane/EtOAc 95:5). ^{1}H NMR (300 MHz, $CDCl_3$) δ (ppm) 9.88 (s, 1H, H_8), 7.83 (d, J = 8.4 Hz, 2H, H_4, H_6), 7.00 (d, J = 8.4 Hz, 2H, H_1, H_3), 3.93 (d, J = 5.7 Hz, 2H, H_{11}), 1.69 (h, J = 6.1 Hz, 1H, H_{12}), 1.52–1.44 (m, 4H, H_{13}, H_{14}), 0.94 (t, J = 7.3 Hz, 6H, H_{15}, H_{16}).

4.5.5. 4-((5-Methylhexyl)oxy)benzaldehyde (14e)

The compound was obtained according to General Procedure A. The product was obtained in pure form, without the need for further purification. Reaction time: 4 h. Starting reagent: 1-bromo-5-methylhexane. Aspect: colorless oil. Yield: 91 %. R_f: 0.67 (cyclohexane/EtOAc 8:2). ^{1}H NMR (300 MHz, $CDCl_3$) δ (ppm) 9.86 (s, 1H, H_8), 7.81 (d, J = 8.4 Hz, 2H, H_4, H_6), 6.97 (d, J = 8.4 Hz, 2H, H_1, H_3), 4.02 (t, J = 6.5 Hz, 2H, H_{11}), 1.87–1.68 (m, 2H, H_{12}), 1.63–1.37 (m, 3H, H_{13}, H_{15}), 1.30–1.15 (m, 2H, H_{14}), 0.88 (d, J = 6.6 Hz, 6H, H_{16}, H_{17}).

4.5.6. 4-(3-(Trifluoromethyl)phenoxy)benzaldehyde (14f)

4-Fluorobelzaldehyde (1.17 mmol, 1 eq) was added at room temperature to a stirred solution of 3-(trifluoromethyl)phenol (1.17 mmol, 1 eq.) and oven-dried K_2CO_3 (2.34 mmol, 2 eq.) in dry DMSO (2 mL). The mixture was stirred for 10 min at 140 °C under a nitrogen atmosphere and microwave irradiation. The reaction mixture was extracted with EtOAc (3 × 5 mL), and the organic phase was washed with cold water, dried over anhydrous Na_2SO_4, filtered, and evaporated *in vacuo*. The resulting solid was purified by flash column chromatography (cyclohexane/EtOAC 85:15) to afford the final product as a pale-yellow oil. Yield: 66 %. R_f: 0.52 (cyclohexane/EtOAc 85:15). ^{1}H NMR (300 MHz, $CDCl_3$) δ (ppm) 9.96 (s, 1H, H_8), 7.89 (d, J = 8.7 Hz, 2H, H_4, H_6), 7.61–7.41 (m, 2H, H_{14}, H_{16}), 7.34 (s, 1H, H_{12}), 7.31–7.20 (m, 1H, H_{15}, partially overlapped with the solvent), 7.10 (d, J = 8.7 Hz, 2H, H_1, H_3).

4.5.7. 4-Phenethoxybenzaldehyde (14g)

The compound was obtained according to General Procedure A. Purification: flash column chromatography (cyclohexane/EtOAc 8:2). Reaction time: 48 h. Starting reagent: (2-bromoethyl)benzene. Aspect: yellow oil. Yield: 70 %. R_f: 0.45 (cyclohexane/EtOAc 8:2). ^{1}H NMR (300 MHz, $CDCl_3$) δ (ppm) 9.88 (s, 1H, H_8), 7.82 (d, J = 8.8 Hz, 2H, H_4, H_6), 7.42–7.17 (m, 5H, H_{14}, H_{15}, H_{16}, H_{17}, H_{18}, partially overlapped with the solvent), 6.99 (d, J = 8.8 Hz, 2H, H_1, H_3), 4.26 (t, J = 7.0 Hz, 2H, H_{11}), 3.13 (t, J = 7.0 Hz, 2H, H_{12}).

4.5.8. 4-(3-Fluorophenethoxy)benzaldehyde (14h)

The compound was obtained according to General Procedure A. Purification: flash column chromatography (cyclohexane/EtOAc 8:2). Reaction time: 48 h. Starting reagent: (1-(2-bromoethyl)-3-fluorobenzene. Aspect: yellow oil. Yield: 70 %. R_f: 0.53 (cyclohexane/EtOAc 8:2). ^{1}H NMR (300 MHz, DMSO-d_6) δ (ppm) 9.84 (s, 1H, H_8), 7.83 (d, J = 8.8 Hz, 2H, H_4, H_6), 7.47–7.26 (m, 1H, H_{17}), 7.24–6.97 (m, 5H, H_1, H_3, H_{14}, H_{16}, H_{18}), 4.32 (t, J = 6.8 Hz, 2H, H_{11}), 3.08 (t, J = 6.8 Hz, 2H, H_{12}).

4.5.9. 4-(3-Phenylpropoxy)benzaldehyde (14i)

The compound was obtained according to General Procedure A. Purification: flash column chromatography (cyclohexane/EtOAc 8:2). Reaction time: 4 h. Starting reagent: (3-bromopropyl)benzene. Aspect: colorless oil. Yield: 91 %. R_f: 0.68 (cyclohexane/EtOAc 8:2). ^{1}H NMR (300 MHz, $CDCl_3$) δ (ppm) 9.88 (s, 1H, H_8), 7.83 (d, J = 8.6 Hz, 2H, H_4, H_6), 7.37–7.15 (m, 5H, H_{15}, H_{16}, H_{17}, H_{18}, H_{19}, partially overlapped with the solvent), 6.98 (d, J = 8.6 Hz, 2H, H_1, H_3), 4.04 (t, J = 6.3 Hz, 2H, H_{11}), 2.83 (t, J = 7.5 Hz, 2H, H_{13}), 2.15 (p, J = 6.6 Hz, 2H, H_{12}).

4.5.10. 2-Methyl-4-(4-(trifluoromethyl)benzylidene)oxazol-5(4H)-one (15a)

General procedure B. A solution of *N*-acetyl-glycine (**13**, 1.71 mmol, 1.1 eq.), the appropriate benzaldehyde (1.55 mmol, 1 eq.), and NaOAc (1.55 mmol, 1 eq.) in acetic anhydride (0.5 mL) was stirred at 100 °C for 5 h. The reaction mixture was purified with the appropriate work-up, depending on the products. For **15a**, the reaction mixture was cooled, and the residue was filtered and washed with MeOH to give the desired product. Starting reagent: 4-(trifluoromethyl)benzaldehyde (**14a**). Aspect: yellow solid. Yield: 60 %. R_f: 0.64 (cyclohexane/EtOAc 8:2). Mp: 138–140 °C. ^{1}H NMR (300 MHz, $CDCl_3$) δ (ppm) 8.19 (d, J = 8.6 Hz, 2H, H_4, H_6), 7.69 (d, J = 8.3 Hz, 2H, H_1, H_3), 7.14 (s, 1H, H_7), 2.44 (s, 3H, H_{14}).

4.5.11. 4-(4-Isobutoxybenzylidene)-2-methyloxazol-5(4H)-one (15b)

The compound was obtained according to general procedure B. Work up: the reaction mixture was extracted with EtOAc (3 × 2 mL). The organic phase was dried over anhydrous Na_2SO_4, filtered, and evaporated *in vacuo*. The crude was purified by flash column chromatography (petroleum ether/EtOAc 95:5). Starting reagent: 4-isobutoxybenzaldehyde (**14b**). Aspect: yellow solid. Yield: 35 %. R_f: 0.56 (petroleum ether/EtOAc 95:5). Mp: 102 °C. ^{1}H NMR (300 MHz, $CDCl_3$) δ (ppm) 8.04 (d, J = 8.9 Hz, 2H, H_4, H_6), 7.11 (s, 1H, H_7), 6.94 (d, J = 8.9 Hz, 2H, H_1, H_3), 3.85–3.65 (m, 2H, H_{16}), 2.39 (s, 3H, H_{14}), 2.11 (hept, J = 6.0 Hz, 1H, H_{17}), 1.04 (d, J = 6.7 Hz, 6H, H_{18}, H_{19}).

4.5.12. 2-Methyl-4-(4-(2-methylbutoxy)benzylidene)oxazol-5(4H)-one (15c)

The compound was obtained according to general procedure B. Work up: the reaction mixture was extracted with EtOAc (3 × 2 mL). The organic phase was dried over anhydrous Na_2SO_4, filtered, and evaporated *in vacuo*. The crude was purified by flash column chromatography (petroleum ether/EtOAc 95:5). Starting reagent: 4-(2- methylbutoxy) benzaldehyde (**14c**). Aspect: yellow oil. Yield: 40 %. R_f: 0.55 (petroleum ether/EtOAc 95:5). ^{1}H NMR (300 MHz, $CDCl_3$) δ (ppm) 8.04 (d, J = 8.8 Hz, 2H, H_4, H_6), 7.10 (s, 1H, H_7), 6.94 (d, J = 8.8 Hz, 2H, H_1, H_3), 3.96–3.70 (m, 2H, H_{16}), 2.39 (s, 3H, H_{14}), 1.99–1.77 (m, 1H, H_{17}), 1.65–1.48 (m, 1H, $H_{18'}$, partially overlapped with H_2O), 1.29–1.19 (m, 1H, $H_{18''}$), 1.02 (d, J = 6.7 Hz, 3H, H_{19}), 0.95 (t, J = 7.4 Hz, 3H, H_{20}).

4.5.13. 4-(4-(2-Ethylbutoxy)benzylidene)-2-methyloxazol-5(4H)-one (15d)

The compound was obtained according to General Procedure B. Work up: the reaction mixture was extracted with EtOAc (3 × 2 mL). The organic phase was dried over anhydrous Na_2SO_4, filtered, and evaporated *in vacuo*. The crude was purified by flash column chromatography

(petroleum ether/EtOAc 95:5). Starting reagent: 4-(2-ethylbutoxy) benzaldehyde (**14d**). Aspect: yellow solid. Yield: 42 %. R_f: 0.48 (petroleum ether/EtOAc 95:5). Mp: 68–70 °C. ^{1}H NMR (300 MHz, $CDCl_3$) δ (ppm) 8.04 (d, $J = 8.9$ Hz, 2H, H_4, H_6), 7.11 (s, 1H, H_7), 6.95 (d, $J = 8.9$ Hz, 2H, H_1, H_3), 3.91 (d, $J = 5.8$ Hz, 2H, H_{16}), 2.39 (s, 3H, H_{14}), 1.68 (h, $J = 6.1$ Hz, 1H, H_{17}), 1.52–1.44 (m, 4H, H_{18}, H_{19}), 0.94 (t, $J = 7.5$ Hz, 6H, H_{20}, H_{21}).

*4.5.14. 2-Methyl-4-(4-((5-methylhexyl)oxy)benzylidene)oxazol-5(4H)-one (**15e**)*

The compound was obtained according to General Procedure B. Work-up: The reaction mixture was extracted with EtOAc (3 × 2 mL). The organic phase was dried over anhydrous Na_2SO_4, filtered, and evaporated *in vacuo*. The crude product was used directly in the next step. Both the product and the starting benzaldehyde exhibited the same R_f value, making purification by flash column chromatography unfeasible. Starting reagent: 4-((5-methylhexyl)oxy)benzaldehyde (**14e**). R_f: 0.55 (cyclohexane/EtOAc 7:3).

*4.5.15. 2-Methyl-4-(4-(3-(trifluoromethyl)phenoxy)benzylidene)oxazol-5(4H)-one (**15f**)*

The compound was obtained according to General Procedure B. Work-up: the reaction mixture was cooled, and the residue was filtered and washed with MeOH. The crude product was used directly in the next step. Both the product and the starting benzaldehyde exhibited the same R_f value, making purification by flash column chromatography unfeasible. Starting reagent: 4-(3-(trifluoromethyl)phenoxy)benzaldehyde (**14f**). R_f: 0.43 (cyclohexane/EtOAc 9:1).

*4.5.16. 2-Methyl-4-(4-phenethoxybenzylidene)oxazol-5(4H)-one (**15g**)*

The compound was obtained according to General Procedure B. Work-up: the reaction mixture was extracted with EtOAc (3 × 2 mL). The organic phase was dried over anhydrous Na_2SO_4, filtered, and evaporated in *vacuo*. The crude product was used directly in the next step. Both the product and the starting benzaldehyde exhibited the same R_f value, making purification by flash column chromatography unfeasible. Starting reagent: 4-phenethoxybenzaldehyde (**14g**). Aspect: yellow solid. R_f: 0.63 (cyclohexane/EtOAc 8:2).

*4.5.17. 4-(4-(3-Fluorophenethoxy)benzylidene)-2-methyloxazol-5(4H)-one (**15h**)*

The compound was obtained according to General Procedure B. Work-up: the reaction mixture was extracted with EtOAc (3 × 2 mL). The organic phase was dried over anhydrous Na_2SO_4, filtered, and evaporated in *vacuo*. The crude product was used directly in the next step. Both the product and the starting benzaldehyde exhibited the same R_f value, making purification by flash column chromatography unfeasible. Starting reagent: 4-(3-fluorophenethoxy)benzaldehyde (**14h**). Aspect: brown oil. R_f: 0.57 (cyclohexane/EtOAc 8:2).

*4.5.18. 2-Methyl-4-(4-(3-phenylpropoxy)benzylidene)oxazol-5(4H)-one (**15i**)*

The compound was obtained according to General Procedure B. Work-up: the reaction mixture was cooled, and the residue was filtered and washed with MeOH to give the desired, pure product. Starting reagent: 4-(3-phenylpropoxy)benzaldehyde (**14i**). Aspect: yellow solid. Yield: 66 %. R_f: 0.72 (cyclohexane/EtOAc 8:2). Mp: 130–132 °C. ^{1}H NMR (300 MHz, $CDCl_3$) δ (ppm) 8.04 (d, $J = 8.8$ Hz, 2H, H_4, H_6), 7.38–7.06 (m, 6H, H_7, H_{20}, H_{21}, H_{22}, H_{23}, H_{24}, and CH, partially overlapped with the solvent), 6.94 (d, $J = 8.8$ Hz, 2H, H_1, H_3), 4.02 (t, $J = 6.3$ Hz, 2H, H_{16}), 2.82 (t, $J = 7.5$ Hz, 2H, H_{18}), 2.38 (s, 3H, H_{14}), 2.20–2.07 (m, 2H, H_{17}).

*4.5.19. 4-(4-Bromobenzylidene)-2-methyloxazol-5(4H)-one (**15l**)*

The compound was obtained according to General Procedure B. Work-up: the reaction mixture was cooled, and the residue was filtered and washed with MeOH to give the desired, pure product. Starting reagent: 4-bromobenzaldehyde (**14l**). Aspect: yellow solid. Yield: 54 %. R_f: 0.53 (cyclohexane/EtOAc 9:1). Mp: 196–198 °C. ^{1}H NMR (300 MHz, $CDCl_3$) δ (ppm) 7.95 (d, $J = 8.6$ Hz, 2H, H_4, H_6), 7.57 (d, $J = 8.6$ Hz, 2H, H_1, H_3), 7.06 (s, 1H, H_7), 2.41 (s, 3H, H_{14}).

*4.5.20. 2-Acetamido-3-(4-(trifluoromethyl)phenyl)acrylic acid (**16a**)*

General procedure C. A solution of the appropriate 4-benzylidene-2-methyloxazol-5(4*H*)-one derivative (**15a-l**, 0.60 mmol) in vinegar (0.6 mL) was stirred at reflux for 3 h. The solid was filtered to afford the desired, pure compound. Starting reagent: 2-methyl-4-(4-(trifluoromethyl)benzylidene)oxazol-5(4*H*)-one (**15a**). Aspect: yellow solid. Yield: 54 %. R_f: 0.29 (DCM/MeOH 9:1). Mp: 156–158 °C. ^{1}H NMR (300 MHz, CD_3OD) δ (ppm) 7.93 (d, $J = 8.3$ Hz, 2H, H_4, H_6), 7.60 (d, $J = 8.3$ Hz, 2H, H_1, H_3), 6.50 (s, 1H, H_8), 2.09 (s, 3H, H_{15}).

*4.5.21. 2-Acetamido-3-(4-isobutoxyphenyl)acrylic acid (**16b**)*

The compound was obtained according to General Procedure C. Aspect: yellow solid. Starting reagent: 4-(4-isobutoxybenzylidene)-2-methyloxazol-5(4*H*)-one (**15b**). Yield: 78 %. Mp: 200–205 °C (dec.). R_f: 0.30 (DCM/MeOH 9:1). ^{1}H NMR (300 MHz, CD_3OD) δ (ppm) 7.55 (d, $J = 8.8$ Hz, 2H, H_4, H_6) 7.47 (s, 1H, H_8), 6.94 (d, $J = 8.8$ Hz, 2H, H_1, H_3), 3.78 (d, $J = 6.5$ Hz, 2H, H_{17}), 2.11 (s, 3H, H_{15}), 2.09–1.98 (m, 1H, H_{18}), 1.03 (d, $J = 6.7$ Hz, 6H, H_{19}, H_{20}).

*4.5.22. 2-Acetamido-3-(4-(2-methylbutoxy)phenyl)acrylic acid (**16c**)*

The compound was obtained according to General Procedure C. Aspect: yellow solid. Starting reagent: 2-methyl-4-(4-(2-methylbutoxy) benzylidene)oxazol-5(4*H*)-one (**15c**). Yield: 53 %. Mp: 154–155 °C. R_f: 0.24 (DCM/MeOH 9:1). ^{1}H NMR (300 MHz, CD_3OD) δ (ppm) 7.55 (d, $J = 8.8$ Hz, 2H, H_4, H_6), 7.47 (s, 1H, H_8), 6.94 (d, $J = 8.8$ Hz, 2H, H_1, H_3), 3.92–3.74 (m, 2H, H_{17}), 2.11 (s, 3H, H_{15}), 1.96–1.74 (m, 1H, H_{18}), 1.74–1.47 (m, 1H, $H_{19'}$), 1.47–1.17 (m, 1H, $H_{19''}$), 1.17–0.82 (m, 6H, H_{20}, H_{21}).

*4.5.23. 2-Acetamido-3-(4-(2-ethylbutoxy)phenyl)acrylic acid (**16d**)*

The compound was obtained according to General Procedure C. Starting reagent: 4-(4-(2-ethylbutoxy)benzylidene)-2-methyloxazol-5(4*H*)-one (**15d**). Aspect: light yellow solid. Yield: 78 %. R_f: 0.29 (DCM/MeOH 9:1). Mp: 165–170 °C (dec). ^{1}H NMR (300 MHz, CD_3OD) δ (ppm) 7.55 (d, $J = 8.9$ Hz, 2H, H_4, H_6), 7.47 (s, 1H, H_8), 6.94 (d, $J = 8.9$ Hz, 2H, H_1, H_3), 3.92 (d, $J = 5.5$ Hz, 2H, H_{17}), 2.11 (s, 3H, H_{15}), 1.64 (h, $J = 12.3$, 6.2 Hz, 1H, H_{18}), 1.57–1.40 (m, 4H, H_{19}, H_{20}), 0.94 (t, $J = 7.4$ Hz, 6H, H_{21}, H_{22}).

*4.5.24. 2-Acetamido-3-(4-((5-methylhexyl)oxy)phenyl)acrylic acid (**16e**)*

The compound was obtained according to General Procedure C. Work up: the reaction mixture was basified with 1 M NaOH and extracted with water (3 × 2 mL). The aqueous phase was acidified with 2 M HCl and extracted with EtOAc (3 × 5 mL). The organic phase was dried over anhydrous Na_2SO_4, filtered, and evaporated *in vacuo*. Starting reagent: 2-methyl-4-(4-((5-methylhexyl)oxy)benzylidene)oxazol-5(4*H*)-one (**15e**). Aspect: white solid. Yield: 40 %. R_f: 0.33 (DCM/MeOH 9:1). Mp: 165–168 °C. ^{1}H NMR (300 MHz, CD_3OD) δ (ppm) 7.53 (d, $J = 8.8$ Hz, 2H, H_4, H_6), 7.44 (s, 1H, H_8), 6.92 (d, $J = 8.8$ Hz, 2H, H_1, H_3), 4.00 (t, $J = 6.4$ Hz, 2H, H_{17}), 2.11 (s, 3H, H_{15}), 1.86–1.67 (m, 2H, H_{18}), 1.67–1.34 (m, 3H, H_{19}, H_{21}), 1.34–1.17 (m, 2H, H_{20}), 0.90 (d, $J = 6.6$ Hz, 6H, H_{22}, H_{23}).

*4.5.25. 2-Acetamido-3-(4-(3-(trifluoromethyl)phenoxy)phenyl)acrylic acid (**16f**)*

The compound was obtained according to General Procedure C. Work up: the reaction mixture was basified with 1 M NaOH and extracted with water (3 × 2 mL). The aqueous phase was acidified with 2 M HCl and extracted with EtOAc (3 × 5 mL). The organic phase was dried over anhydrous Na_2SO_4, filtered, and evaporated *in vacuo*. Starting

reagent: 2-methyl-4-(4-(3-(trifluoromethyl)phenoxy)benzylidene)oxazol-5(4*H*)-one (**15f**). Aspect: yellow solid. Yield: 48 %. R_f: 0.33 (DCM/MeOH 7:3). Mp: 105–107 °C. ^{1}H NMR (300 MHz, CD_3OD) δ (ppm) 7.69–7.53 (m, 3H, H_4, H_6, H_{18}), 7.51–7.41 (m, 2H, H_8, H_{21}), 7.33–7.24 (m, 2H, H_{20}, H_{22}), 7.06 (d, J = 8.7 Hz, 2H, H_1, H_3), 2.10 (s, 3H, H_{15}).

*4.5.26. 2-Acetamido-3-(4-phenethoxyphenyl)acrylic acid (**16g**)*

The compound was obtained according to General Procedure C. Work up: the reaction mixture was basified with 1 M NaOH and extracted with water (3 × 2 mL). The aqueous phase was acidified with 2 M HCl and extracted with EtOAc (3 × 5 mL). The organic phase was dried over anhydrous Na_2SO_4, filtered, and evaporated *in vacuo*. Starting reagent: 2-methyl-4-(4-phenethoxybenzylidene)oxazol-5(4*H*)-one (**15g**). Aspect: white solid. Yield: 52 %. R_f: 0.12 (DCM/MeOH 8:2). Mp: 162 °C. ^{1}H NMR (300 MHz, CD_3OD) δ (ppm) 7.53 (d, J = 8.9 Hz, 2H, H_4, H_6), 7.45 (s, 1H, H_8), 7.34–7.25 (m, 5H, H_{20}, H_{21}, H_{22}, H_{23}, H_{24}), 6.93 (d, J = 8.9 Hz, 2H, H_1, H_3) 4.22 (t, J = 6.8 Hz, 2H, H_{17}), 3.07 (t, J = 6.8 Hz, 2H, CH_{18}), 2.10 (s, 3H, H_{15}).

*4.5.27. 2-Acetamido-3-(4-(3-fluorophenethoxy)phenyl)acrylic acid (**16h**)*

The compound was obtained according to General Procedure C. Work up: the reaction mixture was basified with 1 M NaOH and extracted with water (3 × 2 mL). The aqueous phase was acidified with 2 M HCl and extracted with EtOAc (3 × 5 mL). The organic phase was dried over anhydrous Na_2SO_4, filtered, and evaporated *in vacuo*. Starting reagent: 4-(4-(3-fluorophenethoxy)benzylidene)-2-methyloxazol-5(4*H*)-one (**15h**). Aspect: white solid. Yield: 45 %. R_f: 0.20 (DCM/MeOH 9:1). Mp: 162–163 °C (dec.). ^{1}H NMR (300 MHz, CD_3OD) δ (ppm) 7.53 (d, J = 8.5 Hz, 2H, H_4, H_6), 7.44 (s, 1H, H_8), 7.29 (q, J = 7.5 Hz, 1H, H_{23}), 7.17–7.00 (m, 2H, H_{22}, H_{24}), 7.00–6.85 (m, 3H, H_1, H_3, H_{20}), 4.23 (t, J = 6.5 Hz, 2H, H_{17}), 3.08 (t, J = 6.5 Hz, 2H, H_{18}), 2.09 (s, 3H, H_{15}).

*4.5.28. 2-Acetamido-3-(4-(3-phenylpropoxy)phenyl)acrylic acid (**16i**)*

The compound was obtained according to General Procedure C. Starting reagent: 2-methyl-4-(4-(3-phenylpropoxy)benzylidene)oxazol-5(4*H*)-one (**15i**). Aspect: yellow solid. Yield: 61 %. R_f: 0.27 (DCM/MeOH 9:1). Mp: 162–163 °C. ^{1}H NMR (300 MHz, CD_3OD) δ (ppm) 7.54 (d, J = 8.9 Hz, 2H, H_4, H_6), 7.47 (s, 1H, H_8), 7.31–7.09 (m, 5H, H_{21}, H_{22}, H_{23}, H_{24}, H_{25}), 6.93 (d, J = 8.9 Hz, 2H, H_1, H_3), 3.99 (t, J = 6.2 Hz, 2H, H_{17}), 2.79 (t, J = 7.4 Hz, 2H, H_{19}), 2.21–2.01 (m, 5H, H_{18}, H_{15}).

*4.5.29. 2-Acetamido-3-(4-bromophenyl)acrylic acid (**16l**)*

The compound was obtained according to General Procedure C. Aspect: yellow solid. Starting reagent: 4-(4-bromobenzylidene)-2-methyloxazol-5(4*H*)-one (**15l**). Yield: 80 %. Mp: 216–218 °C (dec.). R_f: 0.13 (DCM/MeOH 8:2). ^{1}H NMR (300 MHz, CD_3OD) δ (ppm) 7.55 (d, J = 8.6 Hz, 2H, H_4, H_6), 7.47 (d, J = 8.6 Hz, 2H, H_1, H_3), 7.41 (s, 1H, H_8), 2.09 (s, 3H, H_{15}).

*4.5.30. Ethyl 2-hydroxy-3-(4-(trifluoromethyl)phenyl)acrylate (**17a**)*

General procedure D. Concentrated HCl (0.70 mL) was added dropwise to a stirred solution of the appropriate 2-acetamido-3-phenylacrylic acid (**16a-l**, 1 eq., 0.37 mmol) in EtOH (0.70 mL), and the reaction mixture was stirred at reflux for 5 h. Then, EtOH was evaporated *in vacuo*, and the resulting mixture was extracted with EtOAc (3 × 5 mL), dried over anhydrous Na_2SO_4, filtered, and evaporated under reduced pressure. The crude was directly used in the next step due to stability issues. Starting reagent: 2-acetamido-3-(4-(trifluoromethyl)phenyl) acrylic acid (**16a**). R_f: 0.70 (cyclohexane/EtOAc 7:3).

*4.5.31. Ethyl 2-hydroxy-3-(4-isobutoxyphenyl)acrylate (**17b**)*

The compound was obtained according to General Procedure D. Starting reagent: 2-acetamido-3-(4-isobutoxyphenyl)acrylic acid (**16b**). R_f: 0.47 (cyclohexane/EtOAc 8:2).

*4.5.32. Ethyl 2-hydroxy-3-(4-(2-methylbutoxy)phenyl)acrylate (**17c**)*

The compound was obtained according to General Procedure D. Starting reagent: 2-acetamido-3-(4-(2-methylbutoxy)phenyl)acrylic acid (**16c**). R_f: 0.54 (cyclohexane/EtOAc 9:1).

*4.5.33. Ethyl 3-(4-(2-ethylbutoxy)phenyl)-2-hydroxyacrylate (**17d**)*

The compound was obtained according to General Procedure D. Starting reagent: 2-acetamido-3-(4-(2-ethylbutoxy)phenyl)acrylic acid (**16d**). R_f: 0.29 (cyclohexane/EtOAc 9:1).

*4.5.34. Ethyl 2-hydroxy-3-(4-((5-methylhexyl)oxy)phenyl)acrylate (**17e**)*

The compound was obtained according to General Procedure D. Starting reagent: 2-acetamido-3-(4-((5-methylhexyl)oxy)phenyl)acrylic acid (**16e**). R_f: 0.46 (cyclohexane/EtOAc 9:1).

*4.5.35. Ethyl 2-hydroxy-3-(4-(3-(trifluoromethyl)phenoxy)phenyl)acrylate (**17f**)*

The compound was obtained according to General Procedure D. Starting reagent: 2-acetamido-3-(4-(3-(trifluoromethyl)phenoxy) phenyl)acrylic acid (**17f**). R_f: 0.45 (cyclohexane/EtOAc 9:1).

*4.5.36. Ethyl 2-hydroxy-3-(4-phenethoxyphenyl)acrylate (**17g**)*

The compound was obtained according to General Procedure D. Starting reagent: 2-acetamido-3-(4-phenethoxyphenyl)acrylic acid (**17g**). R_f: 0.44 (cyclohexane/EtOAc 9:1).

*4.5.37. Ethyl 3-(4-(3-fluorophenethoxy)phenyl)-2-hydroxyacrylate (**17h**)*

The compound was obtained according to General Procedure D. Starting reagent: 2-acetamido-3-(4-(3-fluorophenethoxy)phenyl)acrylic acid (**16h**). R_f: 0.50 (cyclohexane/EtOAc 8:2).

*4.5.38. Ethyl 2-hydroxy-3-(4-(3-phenylpropoxy)phenyl)acrylate (**17i**)*

The compound was obtained according to General Procedure D. Starting reagent: 2-acetamido-3-(4-(3-phenylpropoxy)phenyl)acrylic acid (**16i**). R_f: 0.70 (cyclohexane/EtOAc 8:2).

*4.5.39. Ethyl 3-(4-bromophenyl)-2-hydroxyacrylate (**17l**)*

The compound was obtained according to General Procedure D. Starting reagent: 2-acetamido-3-(4-bromophenyl)acrylic acid (**16l**). R_f: 0.61 (cyclohexane/EtOAc 6:4).

*4.5.40. 3-(Hydroxymethyl)benzaldehyde (**18b**)*

$NaBH_4$ (0.35 eq., 0.26 mmol) was added dropwise to a cooled solution of isophthalaldehyde (1 eq., 0.74 mmol) in dry THF (1 mL) and dry EtOH (0.3 mL). The mixture was stirred at 0 °C for 1 h under a nitrogen atmosphere. After completion, the reaction was quenched with NH_4Cl (4 mL). The solvent was removed *in vacuo*, and the residue was extracted with DCM (3 × 5 mL), dried over anhydrous Na_2SO_4, filtered, and evaporated under reduced pressure. The crude was purified by flash column chromatography (cyclohexane/EtOAc 6:4) to afford the product as a colorless oil. Yield: 40 %. R_f: 0.31 (cyclohexane/EtOAc 6:4). ^{1}H NMR (300 MHz, $CDCl_3$) δ (ppm) 10.04 (s, 1H, H_8), 7.98–7.75 (m, 2H, H_2, H_6), 7.66 (d, J = 7.5 Hz, 1H, H_4), 7.54 (t, J = 7.5 Hz, 1H, H_3), 4.81 (s, 2H, H_{10}).

*4.5.41. 2-(3-Formylphenoxy)acetic acid (**18c**)*

The compound was obtained according to General Procedure A. Purification: flash column chromatography (DCM/MeOH 8:2 + 0.5 % AcOH). Reaction time: 12 h. Starting reagents: bromoacetic acid, and 3-hydroxybenzaldehyde. Aspect: white solid. Yield: 56 %. Mp: 112–113 °C. R_f: 0.26 (DCM/MeOH 8:2). ^{1}H NMR (300 MHz, CD_3OD) δ (ppm) 9.93 (s, 1H, H_8), 7.65–7.33 (m, 3H, H_2, H_4, H_6), 7.33–7.13 (m, 1H, H_3), 4.47 (s, 2H, H_{11}).

*4.5.42. 2-(3-Formylphenoxy)acetonitrile (**18d**)*

The compound was obtained according to General Procedure A.

Purification: flash column chromatography (cyclohexane/EtOAc 7:3). Reaction time: 4 h. Starting reagents: 2-bromoacetonitrile, and 3-hydroxybenzaldehyde. Aspect: colorless oil. Yield: 58 %. R_f: 0.40 (cyclohexane/EtOAc 7:3). ^{1}H NMR (300 MHz, $CDCl_3$) δ (ppm) 10.01 (s, 1H, H_8), 7.69–7.45 (m, 3H, H_2, H_4, H_6), 7.33–7.20 (m, 1H, H_3, partially overlapped with the solvent), 4.85 (s, 2H, H_{11}).

4.5.43. 3-Hydroxy-5-(3-hydroxyphenyl)-4-(4-(trifluoromethyl)phenyl) furan-2(5H)-one (1)

General procedure E. DBU (1.01 eq., 0.75 mmol) was added dropwise to a cold solution of the appropriate ethyl 2-hydroxy-3-phenylacrylate derivative (**17a-l**, 1 eq, 0.74 mmol) and the desired benzaldehyde (**18a-d**, 1.3 eq., 0.96 mmol) in dry DMF (3.1 mL), and the reaction mixture was stirred at 0 °C for 5 h under a nitrogen atmosphere. The resulting solution was then diluted with EtOAc (10 mL) and extracted with water (3 × 15 mL). The aqueous phase was acidified with 3 M HCl and extracted with EtOAc (3 × 20 mL). The organic phase was washed with cold water to remove the residual DMF, dried over anhydrous Na_2SO_4, filtered, and evaporated *in vacuo*. The resulting solid was purified by flash column chromatography (cyclohexane/EtOAc 8:2) to afford the desired product. Aspect: white solid. Starting reagents: ethyl 2-hydroxy-3-(4-(trifluoromethyl)phenyl)acrylate (**17a**), and 3-hydroxybenzaldehyde (**18a**). Yield: 30 %. Mp: 122–124 °C. R_f: 0.15 (cyclohexane/EtOAc 8:2). FTIR (ATR) ν (cm^{-1}) 3289, 2917, 1732, 1616, 1458, 1394, 1321, 1115, 1064, 849, 789. ^{1}H NMR (300 MHz, CD_3OD) δ (ppm) 7.81 (d, $J = 8.1$ Hz, 2H, H_{15}, H_{19}) 7.59 (d, $J = 8.3$ Hz, 2H, H_{16}, H_{18}), 7.18 (t, $J = 7.9$ Hz, 1H, H_{10}), 6.86 (d, $J = 7.6$ Hz, 1H, H_{11}), 6.80–6.70 (m, 2H, H_9, H_{13}), 6.29 (s, 1H, H_5). ^{13}C NMR (75 MHz, Acetone-d_6) δ(ppm) δ 168.34 (C_3), 157.89 (C_{12}), 140.48 (C_8), 137.69 (C_2), 134.61 (C_1), 130.16 (C_{15}, C_{19}), 128.08 (C_{10}, C_{14}, C_{16}, C_{17}, C_{18}) 125.28 (q, C_{21}), 119.32 (C_{11}), 116.59 (C_{13}), 114.55 (C_9), 80.28 (C_5). ^{19}F NMR (282 MHz, CD_3OD) δ (ppm) −64.33 ($C\underline{F}_3$). HRMS (ESI-): *m/z* calc. for $[C_{17}H_{11}F_3O_4]^-$: 336.0609, $[M - H]^-$ *m/z* found: 335.0535; *m/z* calc. for $[C_{34}H_{22}F_6O_8]^-$: 672.1218, $[2M - H]^-$ *m/z* found: 671.1145.

4.5.44. 3-Hydroxy-5-(3-hydroxyphenyl)-4-(4-isobutoxyphenyl)furan-2 (5H)-one (2)

The compound was obtained according to General Procedure E. Purification: flash column chromatography (petroleum ether/EtOAc 7:3). Aspect: white solid. Starting reagents: ethyl 2-hydroxy-3-(4-isobutoxyphenyl)acrylate (**17b**), and 3-hydroxybenzaldehyde (**18a**). Yield: 28 %. Mp: 188–191 °C. R_f: 0.37 (cyclohexane/EtOAc 6:4). FTIR (ATR) ν (cm^{-1}) 3301, 2960, 2920, 2871, 1725, 1604, 1514, 1386, 1253, 1174, 1024, 837, 789, 705. ^{1}H NMR (300 MHz, CD_3OD) δ (ppm) 7.57 (d, $J =$ 8.8 Hz, 2H, H_{15}, H_{19}), 7.16 (t, $J = 7.7$ Hz, 1H, H_{10}), 6.90–6.63 (m, 5H, H_9, H_{11}, H_{13}, H_{16}, H_{18}), 6.17 (s, 1H, H_5), 3.69 (d, $J = 6.5$ Hz, 2H, H_{22}), 1.99 (h, $J = 6.6$ Hz, 1H, H_{23}), 0.99 (d, $J = 6.7$ Hz, 6H, H_{24}, H_{25}). ^{13}C NMR (75 MHz, Acetone-d_6) δ 168.94 (C_3), 159.46 (C_{12}), 157.79 (C_8), 138.53 (C_2), 137.00 (C_1), 129.98 (C_{10}), 129.27 (C_{15}, C_{19}), 128.18 (C_9), 123.14 (C_{11}), 119.37 (C_{14}), 116.30 (C_{13}), 114.38 (C_{16}, C_{18}), 80.22 (C_5), 73.98 (C_{22}), 20.05 (C_{23}), 18.45 (C_{24}, C_{25}). HRMS (ESI-): *m/z* calc. for $[C_{20}H_{20}O_5]^-$: 340.1311, $[M - H]^-$ *m/z* found: 339.1234; *m/z* calc. for $[C_{40}H_{40}O_{10}]^-$: 680.2622, $[2M - H]^-$ *m/z* found: 679.2581.

4.5.45. 3-Hydroxy-5-(3-hydroxyphenyl)-4-(4-(2-methylbutoxy)phenyl) furan-2(5H)-one (3)

The compound was obtained according to General Procedure E. Purification: flash column chromatography (cyclohexane/EtOAc 6:4). Aspect: white solid. Starting reagents: ethyl 2-hydroxy-3-(4-(2-methylbutoxy)phenyl)acrylate (**17c**), and 3-hydroxybenzaldehyde (**18a**). Yield: 30 %. Mp: 175–179 °C. R_f: 0.38 (cyclohexane/EtOAc 6:4). FTIR (ATR) ν (cm^{-1}) 3302, 2961, 2920, 1724, 1604, 1514, 1385, 1255, 838, 791. ^{1}H NMR (300 MHz, $CDCl_3$) δ 7.52 (d, $J = 8.9$ Hz, 2H, H_{10}, H_{14})7.23 (t, $J = 7.9$ Hz, 1H, H_{16}, partially overlapped with the solvent), 6.95 (d, J = 7.7 Hz, 1H, H_{17}), 6.88–6.75 (m, 4H, H_{11}, H_{13}, H_{15}, H_{19}), 6.10 (s, 1H, H_5), 3.84–3.64 (m, 2H, H_{24}), 1.91–1.72 (m, 1H, H_{23}), 1.62–1.42 (m, 1H, $H_{24'}$), 1.32–1.16 (m, 1H, H_{24}), 1.02–0.86 (m, 6H, H_{25}, H_{26}). ^{13}C NMR (75 MHz, Acetone-d_6) δ(ppm) 168.92 (C_3), 159.49 (C_2), 138.51 (C_1), 136.96 (C_8), 129.96 (C_{16}), 129.25 (C_{10},C_{14}), 128.18 (C_{15}), 123.11 (C_{19}), 119.35 (C_9), 116.30 (C_{17}), 114.43 (C_{11}, C_{13}), 80.21 (C_5), 72.45 (C_{21}), 34.56 (C_{23}), 25.79 (C_{24}), 15.78 (C_{26}), 10.63 (C_{25}). HRMS (ESI-): *m/z* calc. for $[C_{21}H_{22}O_5]^-$: 354.1467, $[M - H]^-$ *m/z* found: 353.1390; *m/z* calc. for $[C_{42}H_{44}O_{10}]^-$: 708.2934, $[2M - H]^-$ *m/z* found: 707.2860.

4.5.46. 4-(4-(2-Ethylbutoxy)phenyl)-3-hydroxy-5-(3-hydroxyphenyl) furan-2(5H)-one (4)

The compound was obtained according to General Procedure E. Purification: flash column chromatography (cyclohexane/EtOAc 6:4). Aspect: white solid. Starting reagents: ethyl 3-(4-(2-ethylbutoxy) phenyl)-2-hydroxyacrylate (**17d**), and 3-hydroxybenzaldehyde (**18a**). Yield: 28 %. Mp: 175 °C. R_f: 0.29 (cyclohexane/EtOAc 7:3). FTIR (ATR) ν (cm^{-1}) 3299, 2961, 2927, 2875, 1723, 1603, 1514, 1383, 1252, 838, 788. ^{1}H NMR (300 MHz, Acetone-d_6) δ (ppm) 7.65 (d, $J = 8.9$ Hz, 2H, H_{10}, H_{14}), 7.22 (t, $J = 7.7$ Hz, 1H, H_{16}), 7.02–6.76 (m, 5H, H_{11}, H_{13}, H_{15}, H_{17}, H_{19}), 6.31 (s, 1H, H_5), 3.90 (d, $J = 5.6$ Hz, 2H, H_{21}), 1.63 (h, $J = 6.1$ Hz, 1H, H_{22}), 1.56–1.34 (m, 4H, H_{24}, H_{26}), 0.91 (t, $J = 7.5$ Hz, 6H, H_{25}, H_{27}). ^{13}C NMR (75 MHz, Acetone-d_6) δ 159.57 (C_3), 157.83 (C_{18}), 157.72 (C_{12}), 138.53 (C_8), 137.01 (C_2), 129.99 (C_{16}), 129.27 (C_{10}, C_{14}), 128.20 (C_1), 119.37 (C_9), 116.34 (C_{15}), 116.25 (C_{19}), 114.47 (C_{17}), 114.39 (C_{11}, C_{13}), 80.22 (C_5), 69.73 (C_{21}), 40.82 (C_{22}), 23.10 (C_{24}, C_{26}), 10.47 (C_{25}, C_{27}). HRMS (ESI-): *m/z* calc. for $[C_{22}H_{24}O_5]^-$: 368.1624, $[M - H]^-$ *m/z* found: 367.1545; *m/z* calc. for $[C_{44}H_{48}O_{10}]^-$: 736.3248, $[2M - H]^-$ *m/z* found: 735.3170.

4.5.47. 3-Hydroxy-5-(3-hydroxyphenyl)-4-(4-((5-methylhexyl)oxy) phenyl)furan-2(5H)-one (5)

The compound was obtained according to General Procedure E. Purification: flash column chromatography (cyclohexane/EtOAc 7:3). Aspect: white solid. Starting reagents: ethyl 2-hydroxy-3-(4-((5-methylhexyl)oxy)phenyl)acrylate (**17e**), and 3-hydroxybenzaldehyde (**18a**). Yield: 31 %. Mp: 134–136.7 °C (dec.). R_f: 0.45 (cyclohexane/EtOAc 6:4). FTIR (ATR) ν (cm^{-1}) 3300, 2949, 2867, 1727, 1604, 1514, 1383, 1249, 838, 788. ^{1}H NMR (300 MHz, Acetone-d_6) δ (ppm) 9.16 (s, 1H, br s exch H_2O, OH), 8.43 (s, 1H, br s exch H_2O, OH), 7.65 (d, $J = 8.9$ Hz, 2H, H_{10}, H_{14}), 7.21 (t, $J = 7.7$ Hz, 1H, H_{16}), 7.10–6.68 (m, 5H, H_{Ar} H_{11}, H_{13}, H_{15}, H_{17}, H_{19}), 6.30 (s, 1H, H_5), 3.99 (t, $J = 6.5$ Hz, 2H, H_{21}), 1.73 (p, $J = 6.7$ Hz, 2H, H_{23}), 1.63–1.38 (m, 3H, H_{24}, H_{26}), 1.36–1.14 (m, 2H, H_{25}), 0.87 (d, $J = 7.2$ Hz, 6H, H_{27}, H_{28}). ^{13}C NMR (75 MHz, Acetone-d_6) δ (ppm) 168.93 (C_3), 159.38 (C_{12}), 157.79 (C_{18}), 138.51 (C_8), 136.97 (C_2), 129.97 (C_1), 129.25 (C_{10}, C_{14}) 128.19 (C_{16}), 123.09 (C_9), 119.35 (C_{15}), 116.31 (C_{19}), 114.45 (C_{17}), 114.35 (C_{11}, C_{13}), 80.22 (C_5), 67.67 (C_{21}), 38.47 (C_{25}), 29.24 (C_{23}), 27.74 (C_{27}, C_{28}) 23.60 (C_{24}), 21.95 (C_{26}). HRMS (ESI-): *m/z* calc. for $[C_{23}H_{26}O_5]^-$: 382.1780, $[M - H]^-$ *m/z* found: 381.1703; *m/z* calc. for $[C_{46}H_{52}O_{10}]^-$: 764.3560, $[2M - H]^-$ *m/z* found: 763.3484.

4.5.48. 3-Hydroxy-5-(3-hydroxyphenyl)-4-(4-(3-(trifluoromethyl) phenoxy)phenyl)furan-2(5H)-one (6)

The compound was obtained according to General Procedure E. Purification: flash column chromatography (cyclohexane/EtOAc 7:3). Aspect: white solid. Starting reagents: ethyl 2-hydroxy-3-(4-(3-(trifluoromethyl)phenoxy)phenyl)acrylate (**17f**), and 3-hydroxybenzaldehyde (**18a**). Yield: 35 %. Mp: 109.5–110.5 °C. R_f: 0.33 (cyclohexane/EtOAc 6:4). FTIR (ATR) ν (cm^{-1}) 3301, 2961, 2919, 1729, 1591, 1508, 1449, 1386, 1237, 914, 789, 698. ^{1}H NMR (300 MHz, $CDCl_3$) δ (ppm) 7.58 (d, $J = 8.8$ Hz, 2H, H_{10}, H_{14}), 7.52–7.35 (m, 2H, H_{16}, H_{26}), 7.35–7.12 (m, 3H, partially overlapped with the solvent, H_{23}, H_{25}, H_{27}), 7.17 (d, $J =$ 8.0 Hz, 1H, H_{15}) 7.04–6.89 (m, 3H, H_{11}, H_{13}, H $_{19}$), 6.89–6.74 (m, 2H, H_{17}, H_{22}), 6.20–6.03 (m, 2H, H_5, H_6). ^{13}C NMR (75 MHz, Acetone-d_6) δ (ppm) 168.73 (C $_3$), 157.86 (C $_{21}$), 157.16 (C $_{18}$), 156.49 (C_2, C_{12}) 138.26 (C_8), 138.19 (C_1), 131.94 (C_{24}), 131.17 (C_{26}), 130.08 (C_{16}), 129.67 (C_{10}, C_{14}) 127.13 (C_9), 126.71 (C_{28}), 122.68 (C_{15}), 120.24 (q, C_{25}), 119.35

(C_{27}), 118.74 (C_{11}, C_{13}) 115.46 (C_{17}), 115.63 (q, C_{23}), 114.46 (C_{19}), 80.26 (C_5). ^{19}F NMR (282 MHz, $CDCl_3$) δ (ppm) −62.76 ($C\underline{F}_3$). HRMS (ESI-): *m/z* calc. for $[C_{23}H_{15}F_3O_5]^-$: 428.0872, $[M-H]^-$ *m/z* found: 427.0793.

4.5.49. 3-Hydroxy-5-(3-hydroxyphenyl)-4-(4-phenethoxyphenyl)furan-2(5H)-one (7)

The compound was obtained according to General Procedure E. Purification: flash column chromatography (cyclohexane/EtOAc 6:4). Aspect: white solid. Starting reagents: ethyl 2-hydroxy-3-(4-phenethoxyphenyl)acrylate (**17g**), and 3-hydroxybenzaldehyde (**18a**). Yield: 25 %. Mp: 158–160 °C. R_f: 0.49 (cyclohexane/EtOAc 6:4). FTIR (ATR) ν (cm^{-1}) 3297, 3060, 2920, 1721, 1602, 1512, 1383, 1249, 839, 700. ^{1}H NMR (300 MHz, Acetone-d_6) δ (ppm) 7.65 (d, $J = 8.7$ Hz, 2H, H_{10}, H_{14}), 7.40–7.13 (m, 6H, H_{19}, H_{25}, H_{26}, H_{27}, H_{28}, H_{29}), 7.00–6.76 (m, 5H, H_{11}, H_{13}, H_{15}, H_{16}, H_{17}), 6.30 (s, 1H, H_5), 4.20 (t, $J = 6.9$ Hz, 2H, H_{21}), 3.06 (t, $J = 6.9$ Hz, 2H, H_{23}). ^{13}C NMR (75 MHz, Acetone-d_6) δ (ppm) 168.93 (C_3), 159.06 (C_{12}), 157.79 (C_{18}), 138.49 (C_{24}), 138.43 (C_8), 137.08 (C_2), 129.98 (C_1), 129.27 (C_{10}, C_{14}), 128.96 (C_{25}, C_{29}), 128.31 (C_{26}), 128.28 (C_{28}), 128.11 (C_{11}), 126.27 (C_{27}), 123.30 (C_9), 119.36 (C_{15}), 116.32 (C_{17}), 114.45, (C_{19}) 114.43 (C_{11},C_{13}), 80.22 (C_5), 68.42 (C_{21}), 35.30 (C_{23}). HRMS (ESI-): *m/z* calc. for $[C_{24}H_{20}O_5]^-$: 388.1311, $[M-H]^-$ *m/z* found: 387.1233; *m/z* calc. for $[C_{48}H_{40}O_{10}]^-$: 776.2622, $[2M-H]^-$ *m/z* found: 775.2544.

4.5.50. 4-(4-(3-Fluorophenethoxy)phenyl)-3-hydroxy-5-(3-hydroxyphenyl)furan-2(5H)-one (8)

The compound was obtained according to General Procedure E. Purification: flash column chromatography (cyclohexane/EtOAc 6:4). Aspect: white solid. Starting reagents: ethyl 3-(4-(3-fluorophenethoxy) phenyl)-2-hydroxyacrylate (**17h**), and 3-hydroxybenzaldehyde (**18a**). Yield: 20 %. Mp: 187–191 °C. R_f: 0.46 (cyclohexane/EtOAc 6:4). FTIR (ATR) ν (cm^{-1}) 3303, 2960, 2922, 1723, 1604, 1513, 1383, 1255, 839, 787, 692. ^{1}H NMR (300 MHz, CD_3OD) δ (ppm) 7.58 (d, $J = 8.8$ Hz, 2H, H_{10}, H_{14}), 7.27 (q, $J = 7.8$ Hz, 1H, H_{28}), 7.16 (t, $J = 7.8$ Hz, 1H, H_{16}), 7.12–6.97 (m, 2H, H_{25}, H_{29}), 6.96–6.65 (m, 6H, H_{11}, H_{13}, H_{15}, H_{17}, H_{19}, H_{27}), 6.17 (s, 1H, H_5), 4.16 (t, $J = 6.6$ Hz, 2H, H_{21}), 3.04 (t, $J = 6.6$ Hz, 2H, H_{23}). ^{13}C NMR (75 MHz, Acetone-d_6) δ (ppm) 168.89 (C_3), 164.39 (C_{12}), 161.16 (C_{18}), 158.96 (C_{26}), 141.51 (C_{24}), 141.41 (C_8), 138.47 (C_2), 137.09 (C_1), 129.93 (C_{28}), 129.27 (C_{10},C_{14}), 128.06 (C_{25}), 124.97 (C_{29}), 123.39 (C_9), 119.35 (C_{17}), 116.31 (C_{15}), 115.77 (C_{19}), 115.49, 114.42 (C_{11},C_{13}), 113.09 (C_{27}), 80.20 (C_5), 67.98 (C_{21}), 34.90 (C_{23}). HRMS (ESI-): *m/z* calc. for $[C_{24}H_{19}FO_5]^-$: 406.1217, $[M-H]^-$ *m/z* found: 405.1139.

4.5.51. 3-Hydroxy-5-(3-hydroxyphenyl)-4-(4-(3-phenylpropoxy)phenyl)furan-2(5H)-one (9)

The compound was obtained according to General Procedure E. Purification: flash column chromatography (cyclohexane/EtOAc 6:4). Aspect: white solid. Starting reagents: ethyl 2-hydroxy-3-(4-(3-phenylpropoxy)phenyl)acrylate (**17i**), and 3-hydroxybenzaldehyde (**18a**). Yield: 40 %. Mp: 158–160 °C. R_f: 0.45 (cyclohexane/EtOAc 6:4). FTIR (ATR): ν (cm^{-1}) 3295, 3025, 2918, 1723, 1603, 1513, 1382, 1252, 839, 789, 700. ^{1}H NMR (300 MHz, Acetone-d_6) δ (ppm) 7.65 (d, $J = 9.0$ Hz, 2H, H_{10}, H_{14}), 7.31–7.14 (m, 6H, H_{16}, H_{17}, H_{19}, H_{27}, H_{28}, H_{29}), 7.06–6.74 (m, 5H, H_{11}, H_{13}, H_{15}, H_{26}, H_{30}), 6.30 (s, 1H, H_5), 3.99 (t, $J =$ 6.3 Hz, 2H, H_{21}), 2.78 (t, $J = 7.0$ Hz, 2H, H_{24}), 2.14–1.92 (m, 2H, CH_2–$\underline{CH}_2$–CH_2, partially overlapped with the solvent, H_{23}). ^{13}C NMR (75 MHz, Acetone-d_6) δ (ppm) 169.01 (C_3), 159.26 (C_{12}), 157.80 (C_{18}), 141.59 (C_{25}), 138.51 (C_2), 137.11 (C_8), 129.98 (C_1), 129.26 (C_{10}, C_{14}), 128.38 (C_{26}, C_{30}), 128.29 (C_{27},C_{29}), 128.10 (C_{16}), 125.78 (C_{28}), 123.25 (C_9), 119.35 (C_{15}), 116.32 (C_{17}), 114.46 (C_{19}), 114.39 (C_{11}, C_{13}), 80.24 (C_5), 66.78 (C_{21}), 31.74 (C_{24}), 30.75 (C_{23}). HRMS (ESI-): *m/z* calc. for $[C_{25}H_{22}O_5]^-$: 402.1467, $[M-H]^-$ *m/z* found: 401.1390.

4.5.52. 4-(4-Bromophenyl)-3-hydroxy-5-(3-(hydroxymethyl)phenyl)furan-2(5H)-one (10)

The compound was obtained according to General Procedure E. Purification: flash column chromatography (petroleum ether/EtOAc 7:3). Aspect: white solid. Starting reagents: ethyl 3-(4-bromophenyl)-2-hydroxyacrylate (**17l**), and 3-(hydroxymethyl)benzaldehyde (**18b**). Yield: 28 %. Mp: 205 °C. R_f: 0.31 (petroleum ether/EtOAc 7:3). FTIR (ATR) ν (cm^{-1}) 3305, 2916, 2850, 1733, 1487, 1383, 1143, 1009, 796, 704. ^{1}H NMR (300 MHz, CD_3OD) δ (ppm) 7.58–7.52 (m, 2H, H_5, H_3), 7.47–7.40 (m, 2H, H_2, H_6), 7.36–7.34 (m, 3H, H_{15}, H_{17}, H_{19}), 7.31–7.25 (m, 1H, H_{16}), 6.34 (s, 1H, H_{11}), 4.57 (s, 2H, H_{20}). ^{13}C NMR (75 MHz, DMSO-d_6) δ (ppm) 169.35 (C_9), 143.93 (C_{18}), 139.85 (C_{14}), 136.57 (C_8), 131.95 (C_{26}), 130.18 (C_7), 129.60 (C_3, C_5), 129.11 (C_4), 127.86 (C_{16}), 127.05 (C_{19}), 126.91 (C_{15}), 125.65 (C_{17}), 121.99 (C_1), 80.08 (C_{11}), 62.89 (C_{20}). HRMS (ESI-): *m/z* calc. for $[C_{17}H_{13}BrO_4]^-$: 359.9997, $[M-H]^-$ *m/z* found: 358.9921.

4.5.53. 2-(3-(3-(4-Bromophenyl)-4-hydroxy-5-oxo-2,5-dihydrofuran-2-yl)phenoxy)acetic acid (11)

The compound was obtained according to General Procedure E. Purification: crystallization from MeOH/hexane. Aspect: white solid. Starting reagents: ethyl 3-(4-bromophenyl)-2-hydroxyacrylate (**17l**), and 2-(3-formylphenoxy)acetic acid (**18c**). Yield: 58 %. Mp: 230–232 °C (dec.). R_f: 0.20 (DCM/cyclohexane 8:2). FTIR (ATR) ν (cm^{-1}) 3208, 2920, 1729, 1589, 1489, 1382, 1160, 1073, 1009, 838, 794, 703. ^{1}H NMR (300 MHz, DMSO-d_6) δ (ppm) 7.58–7.49 (m, 4H, H_2, H_3, H_5, H_6) 7.25 (t, $J = 8.0$ Hz, 1H, H_{16}), 7.03–6.94 (m, 1H, H_{19}), 6.94–6.82 (m, 2H, H_{15}, H_{17}), 6.49 (s, 1H, H_{11}), 4.64 (s, 2H, H_{22}). ^{13}C NMR (75 MHz, DMSO-d_6) δ (ppm) 170.41 (C_{23}), 169.26 (C_9), 158.39 (C_{18}), 139.76 (C_8), 138.23 (C_{14}), 131.96 (C_2, C_6), 130.58 (C_7), 130.09 (C_4), 129.60 (C_3, C_5), 127.07 (C_{16}), 122.06 (C_1), 120.47 (C_{15}), 115.43 (C_{17}), 115.06 (C_{19}), 79.70 (C_{11}), 64.92 (C_{22}). HRMS (ESI-): *m/z* calc. for $[C_{18}H_{13}BrO_6]^-$: 403.9896, $[M-H]^-$ *m/z* found: 402.9819.

4.5.54. 2-(3-(3-(4-Bromophenyl)-4-hydroxy-5-oxo-2,5-dihydrofuran-2-yl)phenoxy)acetonitrile (12)

The compound was obtained according to General Procedure E. Purification: flash column chromatography (petroleum ether/EtOAc 7:3). Aspect: white solid. Starting reagents: ethyl 3-(4-bromophenyl)-2-hydroxyacrylate (**17l**), and 2-(3-formylphenoxy)acetonitrile (**18d**). Yield: 20 %. Mp: 169–172 °C. R_f: 0.31 (cyclohexane/EtOAc 7:3). FTIR (ATR) ν (cm^{-1}) 3289, 2923, 1738, 1588, 1488, 1384, 1291, 1159, 1009, 877, 837, 791, 702. ^{1}H NMR (300 MHz, Acetone-d_6) δ (ppm) 7.65 (d, J = 8.6 Hz, 2H, H_2, H_6), 7.53 (d, $J = 8.6$ Hz, 2H, H_3, H_5), 7.40 (t, $J = 7.9$ Hz, 1H, H_{16}), 7.26–7.05 (m, 3H, H_{15}, H_{17}, H_{19}), 6.46 (s, 1H, H_{11}), 5.11 (s, 2H, H_{22}). ^{13}C NMR (75 MHz, Acetone-d_6) δ (ppm) 168.47 (C_9), 157.22 (C_{18}), 139.47 (C_{14}), 138.52 (C_8), 131.60 (C_2, C_6), 130.47 (C_4), 129.78 (C_7), 129.38 (C_3, C_5), 126.30 (C_{16}), 122.04 (C_1), 122.00 (C_{15}), 115.69 (C_{17}), 115.64 (C_{23}), 114.91 (C_{19}), 79.83 (C_{11}), 53.44 (C_{22}). HRMS (ESI-): *m/z* calc. for $[C_{18}H_{12}BrNO_4]^-$: 384.9950, $[M-H]^-$ *m/z* found: 383.9873.

4.6. GCI analyses

GCI analyses were performed using a Creoptix WAVE Grating-Coupled Interferometry (GCI) instrument (Malvern Panalytical, Wädenswil, Switzerland) controlled by a Creoptix WAVEcontrol software (4.3.4 version). The running buffer was composed of 10 mM HEPES, pH 7.4, 150 mM NaCl, with 1 % DMSO for kinetic analyses. A constant flow rate of 10 μL/min (immobilization) or 50 μL/min (kinetic analyses) was applied.

The human PPARγ ligand binding domain (LBD) was covalently immobilized on a 4PCH sensor chip functionalized with a high capacity polycarboxylate layer. The immobilization was carried out by amine coupling. The activation step was performed by injecting a mixture of 200 mM EDC and 50 mM NHS for 420 s. A 100 μg/mL PPARγ solution in 20 mM sodium acetate buffer, pH 4.5 was injected (600 s) two times on

one of the chip channels for the immobilization; a second channel was used as a reference. Passivation of the unreacted groups on the chip surface was achieved by a 300 s injection of 1 M ethanolamine, pH 8.0.

For kinetic analyses, a concentration range of 78.125 nM-10 μM was considered, with a dilution factor of 2, an association time of 120 s and a dissociation time of 180 s. A 5-point DMSO calibration curve was built for each analysis in the concentration range 0.5 %–1.5 % DMSO.

4.7. Protein expression and purification

PPARγ-LBD was expressed as an N-terminal His-tagged protein using a pET-28a(+) vector and then purified as previously described [47]. Briefly, freshly transformed *E. coli* BL21(DE3) were grown in LB medium with 50 μg mL^{-1} of kanamycin at 37 °C to an OD_{600} of 0.7. The culture was then induced with 0.2 mM isopropyl-*β*-D-thio-galactopyranoside (IPTG) and further incubated at 18 °C for 20 h. Cells were harvested and resuspended in Buffer A (20 mM Tris, pH 8.0, 150 mM NaCl, 1 mM TCEP, 10 mM imidazole, 10 % *v/v* glycerol) in the presence of protease inhibitors (Complete Tablets EDTA-free; Roche Applied Science, Penzberg, Germany). Cells were sonicated, and the soluble fraction was isolated by centrifugation. The supernatant was loaded onto a nickel-NTA agarose bulk resin (ABT) and eluted with a gradient of imidazole 10–300 mM in Buffer A (batch method). The pure protein was identified by SDS-PAGE. The protein was dialyzed against buffer A to remove imidazole, then the His-tag was cleaved using thrombin protease (GE Healthcare, Chicago, IL, USA) at a ratio of 10 units/mg at room temperature for 2 h. The digested mixture was reloaded onto a Ni^{2+}-NTA column to remove the cleaved His-tag and any undigested protein. The flow-through was dialyzed against buffer B (20 mM Tris, pH 8.0, 1 mM TCEP, 10 % *v/v* glycerol, 1 mM TCEP) and then loaded onto a Q-Sepharose HP column (GE Healthcare) and eluted with a gradient of NaCl 0–500 mM in Buffer B using a BioLogic DuoFlow FPLC system (Bio-Rad Laboratories, Hercules, CA, USA). Finally, PPARγ-LBD was purified by gel filtration on a Superdex 75 column (GE Healthcare) and eluted with Buffer C (20 mM Tris, pH 8.0, 1 mM TCEP, 0.5 mM EDTA). For crystallization, the protein was concentrated at 8 mg mL^{-1} using Amicon centrifugal concentrators with a 10 kDa cutoff membrane (Millipore, Burlington, MA, USA).

4.8. Crystallization, data collection, and structure determination

Crystals of apo-PPARγ-LBD were obtained by vapor diffusion at 20 °C using a sitting drop formed by mixing 2 μL of protein solution with 2 μL of reservoir solution (0.8 M Na citrate, 0.15 M Tris, pH 8.0). The crystals were soaked for 3 days in storage solutions (1.2 M Na citrate, 0.15 M Tris, pH 8.0) containing the ligand at a final concentration of 0.5 mM. The ligand dissolved in DMSO (50 mM) was diluted in the storage solution so that the final concentration of DMSO was 2.5 %. The storage solution with glycerol 20 % (*v/v*) was used as a cryoprotectant. PPARγ-LBD crystallized in the space group C2; cell parameters are shown in Table S1 of the Supporting Materials. X-ray data of PPARγ-LBD in complex with compound **11** were collected at 100 K under a nitrogen stream using synchrotron radiation (beamline ID30A-3 at ESRF, Grenoble, France). The diffracted intensities were processed using the software autoPROC [48]. Structure solution was performed with AMoRe [49], using the coordinates of PDB ID 4YT1 as the starting model. The coordinates were then refined with CNS [50,51] and PHENIX [52] including data between 50.79 and 2.85 Å. The statistics of crystallographic data and refinement are summarized in Table 4. The structure of PPARγ-LBD/**11** complex was deposited in the Protein Data Bank with ID 9HX2.

CRediT authorship contribution statement

Giulia Cazzaniga: Writing – review & editing, Writing – original draft, Methodology, Investigation, Conceptualization. **Davide Capelli:** Writing – review & editing, Writing – original draft, Resources, Methodology, Investigation. **Roberta Montanari:** Writing – review & editing, Resources, Investigation. **Enrico Mario Alessandro Fassi:** Writing – review & editing, Writing – original draft, Methodology, Investigation. **Giovanni Grazioso:** Writing – review & editing, Resources, Investigation. **Andrea Tresoldi:** Investigation. **Francesca Rinaldi:** Writing – review & editing, Writing – original draft, Methodology, Investigation. **Enrica Calleri:** Writing – review & editing, Resources, Methodology, Investigation, Conceptualization. **Ivan Bassanini:** Writing – review & editing, Resources, Methodology. **Sergio Romeo:** Writing – review & editing, Resources. **Mariangela Garofalo:** Writing – review & editing, Methodology, Investigation. **Matteo Mori:** Writing – review & editing, Writing – original draft, Methodology, Investigation, Conceptualization. **Fiorella Meneghetti:** Writing – review & editing, Supervision, Resources. **Stefania Villa:** Writing – review & editing, Supervision, Resources, Conceptualization.

Associated content

The following content is available in the Supporting Information: cytotoxicity assays, MM-GBSA calculations, analytical data, GCI assays.

CCDC accession code 2400627 contains the supplementary crystallographic data for this paper. This data can be obtained free of charge via www.ccdc.cam.ac.uk/data_request/cif, or by emailing data_request@ccdc.cam.ac.uk, or by contacting The Cambridge Crystallographic Data Centre, 12 Union Road, Cambridge CB2 1EZ, UK; fax: +44 1223 336033.

Declaration of competing interest

The authors declare that they have no known competing financial interests or personal relationships that could have appeared to influence the work reported in this paper.

Acknowledgments

F.M. and M.M. thank Prof. Diego Gatta and Dr. Nicola Rotiroti for granting access to their instrument and for their kind support. G.C., M. M., and S.V. are grateful to Prof. Silvia Gazzola for providing access to her instrument. G.C., M.M., and S.V extend their thanks to Martina Quaglia, Carola Gaffuri, and Nadia Zanoni for their valuable contributions.

Appendix A. Supplementary data

Supplementary data to this article can be found online at https://doi.org/10.1016/j.ejmech.2025.117657.

Abbreviations

CCDC	Cambridge Crystallographic Data Centre;
CDK5	cyclin-dependent kinase 5
CSD	Cambridge Structural Database
DBU	1,5-diazabiciclo(5.4.0)undec-7-ene
EDC	1-ethyl-3-(3-dimethylaminopropyl)carbodiimide
GCI	grating-coupled interferometry
HPLC: high-performance liquid chromatography	
HS	Hirshfeld surface
IR	insulin resistance
K_D	dissociation constant
LBD	ligand-binding domain
MD	molecular dynamics
MM-GBSA	molecular mechanics-generalized Born surface area
mp	melting point
NHS	*N*-hydroxysuccinimide
PDB	Protein Data Bank

PPARγ	peroxisome proliferator-activated receptor γ
PTM	post-translational modifications
RMSD	root-mean-square-deviation
RMSF	root-mean-square-fluctuation
RP-HPLC	reversed-phase high-performance liquid chromatography
SC-XRD	single-crystal X-ray diffraction
SPPARγMs	selective PPARγ modulators
SPR	surface plasmon resonance
T2DM	type 2 diabetes mellitus
TLC	thin-layer chromatography
tR	retention time
TZD	thiazolidinediones
XP	extra-precision

Data availability

Data will be made available on request.

References

[1] Y.F. Guan, C. Hao, D.R. Cha, R. Rao, W. Lu, D.E. Kohan, M.A. Magnuson, R. Redha, Y. Zhang, M.D. Breyer, Thiazolidinediones expand body fluid volume through PPARγ stimulation of ENaC-mediated renal salt absorption, Nat. Med. 11 (2005) 861–866, https://doi.org/10.1038/nm1278.

[2] P.D. Home, S.J. Pocock, H. Beck-Nielsen, P.S. Curtis, R. Gomis, M. Hanefeld, N. P. Jones, M. Komajda, J.J. McMurray, Rosiglitazone evaluated for cardiovascular outcomes in oral agent combination therapy for type 2 diabetes (RECORD): a multicentre, randomised, open-label trial, Lancet 373 (2009) 2125–2135, https://doi.org/10.1016/S0140-6736(09)60953-3.

[3] K.R. Shockley, O.P. Lazarenko, P.J. Czernik, C.J. Rosen, G.A. Churchill, B. Lecka-Czernik, PPARγ2 nuclear receptor controls multiple regulatory pathways of osteoblast differentiation from marrow mesenchymal stem cells, J. Cell. Biochem. 106 (2009) 232–246, https://doi.org/10.1002/JCB.21994.

[4] W. Wei, X. Wang, M. Yang, L.C. Smith, P.C. Dechow, Y. Wan, PGC1beta mediates PPARgamma activation of osteoclastogenesis and rosiglitazone-induced bone loss, Cell Metab. 11 (2010) 503–516, https://doi.org/10.1016/J.CMET.2010.04.015.

[5] A. Zieleniak, M. Wójcik, L.A. Woźniak, Structure and physiological functions of the human peroxisome proliferator-activated receptor γ, Arch. Immunol. Ther. Exp. 56 (2008) 331–345, https://doi.org/10.1007/S00005-008-0037-Y/METRICS.

[6] S.H. Han, M.J. Quon, J.a. Kim, K.K. Koh, Adiponectin and cardiovascular disease: response to therapeutic interventions, J. Am. Coll. Cardiol. 49 (2007) 531–538, https://doi.org/10.1016/J.JACC.2006.08.061.

[7] J.B. Bruning, M.J. Chalmers, S. Prasad, S.A. Busby, T.M. Kamenecka, Y. He, K. W. Nettles, P.R. Griffin, Partial agonists activate PPARgamma using a helix 12 independent mechanism, Structure 15 (2007) 1258–1271, https://doi.org/10.1016/J.STR.2007.07.014.

[8] J.H. Choi, A.S. Banks, J.L. Estall, S. Kajimura, P. Boström, D. Laznik, J.L. Ruas, M. J. Chalmers, T.M. Kamenecka, M. Blüher, P.R. Griffin, B.M. Spiegelman, Anti-diabetic drugs inhibit obesity-linked phosphorylation of PPARγ by Cdk5, Nature 466 (2010) 451–456, https://doi.org/10.1038/nature09291.

[9] J.H. Choi, A.S. Banks, T.M. Kamenecka, S.A. Busby, M.J. Chalmers, N. Kumar, D. S. Kuruvilla, Y. Shin, Y. He, J.B. Bruning, D.P. Marciano, M.D. Cameron, D. Laznik, M.J. Jurczak, S.C. Schürer, D. Vidović, G.I. Shulman, B.M. Spiegelman, P.R. Griffin, Antidiabetic actions of a non-agonist PPARγ ligand blocking Cdk5-mediated phosphorylation, Nature 477 (2011) 477–481, https://doi.org/10.1038/nature10383.

[10] A.A. Amato, S. Rajagopalan, J.Z. Lin, B.M. Carvalho, A.C.M. Figueira, J. Lu, S. D. Ayers, M. Mottin, R.L. Silveira, P.C.T. Souza, R.H.V. Mourão, M.J.A. Saad, M. Togashi, L.A. Simeoni, D.S.P. Abdalla, M.S. Skaf, I. Polikparpov, M.C.A. Lima, S. L. Galdino, R.G. Brennan, J.D. Baxter, I.R. Pitta, P. Webb, K.J. Phillips, F.A. R. Neves, GQ-16, a novel peroxisome proliferator-activated receptor γ (PPARγ) ligand, promotes insulin sensitization without weight gain, J. Biol. Chem. 287 (2012) 28169–28179, https://doi.org/10.1074/JBC.M111.332106.

[11] J.C. De Groot, C. Weidner, J. Krausze, K. Kawamoto, F.C. Schroeder, S. Sauer, K. Büssow, Structural characterization of amorfrutins bound to the peroxisome proliferator-activated receptor γ, J. Med. Chem. 56 (2013) 1535–1543, https://doi.org/10.1021/JM3013272.

[12] G. Pochetti, N. Mitro, A. Lavecchia, F. Gilardi, N. Besker, E. Scotti, M. Aschi, N. Re, G. Fracchiolla, A. Laghezza, P. Tortorella, R. Montanari, E. Novellino, F. Mazza, M. Crestani, F. Loiodice, Structural insight into peroxisome proliferator-activated receptor γ binding of two ureidofibrate-like enantiomers by molecular dynamics, cofactor interaction analysis, and site-directed mutagenesis, J. Med. Chem. 53 (2010) 4354–4366, https://doi.org/10.1021/JM9013899.

[13] A. Laghezza, R. Montanari, A. Lavecchia, L. Piemontese, G. Pochetti, V. Iacobazzi, V. Infantino, D. Capelli, M. De Bellis, A. Liantonio, S. Pierno, P. Tortorella, D. Conte Camerino, F. Loiodice, On the metabolically active form of metaglidasen: improved synthesis and investigation of its peculiar activity on peroxisome proliferator-activated receptors and skeletal muscles, ChemMedChem 10 (2015) 555–565, https://doi.org/10.1002/CMDC.201402462.

[14] D.P. Marciano, D.S. Kuruvilla, S.V. Boregowda, A. Asteian, T.S. Hughes, R. Garcia-Ordonez, C.A. Corzo, T.M. Khan, S.J. Novick, H. Park, D.J. Kojetin, D.G. Phinney, J. B. Bruning, T.M. Kamenecka, P.R. Griffin, Pharmacological repression of PPARγ promotes osteogenesis, Nat. Commun. 6 (2015) 1–7, https://doi.org/10.1038/ncomms8443.

[15] D.P. Marciano, D.S. Kuruvilla, B.D. Pascal, P.R. Griffin, Identification of bexarotene as a PPAR γ antagonist with HDX, PPAR Res. 2015 (2015) 254560, https://doi.org/10.1155/2015/254560.

[16] S.S. Choi, E.S. Kim, J.E. Jung, D.P. Marciano, A. Jo, J.Y. Koo, S.Y. Choi, Y.R. Yang, H.J. Jang, E.K. Kim, J. Park, H.M. Kwon, I.H. Lee, S.B. Park, K.J. Myung, P.G. Suh, P.R. Griffin, J.H. Choi, PPARγ antagonist gleevec improves insulin sensitivity and promotes the browning of white adipose tissue, Diabetes 65 (2016) 829–839, https://doi.org/10.2337/DB15-1382.

[17] A. Asteian, A.L. Blayo, Y. He, M. Koenig, Y. Shin, D.S. Kuruvilla, C.A. Corzo, M. D. Cameron, L. Lin, C. Ruiz, S. Khan, N. Kumar, S. Busby, D.P. Marciano, R. D. Garcia-Ordonez, P.R. Griffin, T.M. Kamenecka, Design, synthesis, and biological evaluation of indole biphenylcarboxylic acids as PPARγ antagonists, ACS Med. Chem. Lett. 6 (2015) 998–1003, https://doi.org/10.1021/ACSMEDCHEMLETT.5B00218.

[18] G. Brusotti, R. Montanari, D. Capelli, G. Cattaneo, A. Laghezza, P. Tortorella, F. Loiodice, F. Peiretti, B. Bonardo, A. Paiardini, E. Calleri, G. Pochetti, Betulinic acid is a PPARγ antagonist that improves glucose uptake, promotes osteogenesis and inhibits adipogenesis, Sci. Rep. 7 (2017) 1–14, https://doi.org/10.1038/s41598-017-05666-6.

[19] S.S. Choi, E.S. Kim, M. Koh, S.J. Lee, D. Lim, Y.R. Yang, H.J. Jang, K.A. Seo, S. H. Min, I.H. Lee, S.B. Park, P.G. Suh, J.H. Choi, A novel non-agonist peroxisome proliferator-activated receptor γ (PPARγ) ligand UHC1 blocks PPARγ phosphorylation by cyclin-dependent kinase 5 (CDK5) and improves insulin sensitivity, J. Biol. Chem. 289 (2014) 26618–26629, https://doi.org/10.1074/JBC.M114.566794.

[20] B.L. McVicker, R.L. Simpson, F.G. Hamel, R.G. Bennett, Reduction in obesity-related hepatic fibrosis by SR1664, Biology 12 (2023) 1287, https://doi.org/10.3390/BIOLOGY12101287/S1.

[21] R. Montanari, D. Capelli, K. Yamamoto, H. Awaishima, K. Nishikata, A. Barendregt, A.J.R. Heck, F. Loiodice, F. Altieri, A. Paiardini, A. Grottesi, L. Pirone, E. Pedone, F. Peiretti, J.M. Brunel, T. Itoh, G. Pochetti, Insights into pparγphosphorylation and its inhibition mechanism, J. Med. Chem. 63 (2020) 4811–4823, https://doi.org/10.1021/ACS.JMEDCHEM.0C00048.

[22] T.S. Hughes, M.J. Chalmers, S. Novick, D.S. Kuruvilla, M.R. Chang, T. M. Kamenecka, M. Rance, B.A. Johnson, T.P. Burris, P.R. Griffin, D.J. Kojetin, Ligand and receptor dynamics contribute to the mechanism of graded PPARγ agonism, Structure 20 (2012) 139–150, https://doi.org/10.1016/J.STR.2011.10.018.

[23] D. Capelli, G. Cazzaniga, M. Mori, A. Laghezza, F. Loiodice, M. Quaglia, E. Negro, F. Meneghetti, S. Villa, R. Montanari, Biological screening and crystallographic studies of hydroxy γ-Lactone derivatives to investigate PPARγ phosphorylation inhibition, Biomolecules 13 (2023) 694, https://doi.org/10.3390/BIOM13040694/S1.

[24] S. Ahn, D.M. Jang, S.C. Park, S. An, J. Shin, B.W. Han, M. Noh, Cyclin-dependent kinase 5 inhibitor butyrolactone I elicits a partial agonist activity of peroxisome proliferator-activated receptor γ, Biomolecules 10 (2020) 275, https://doi.org/10.3390/BIOM10020275.

[25] S. Parsons, H.D. Flack, T. Wagner, Use of intensity quotients and differences in absolute structure refinement, Acta Crystallogr B Struct Sci Cryst Eng Mater 69 (2013) 249–259, https://doi.org/10.1107/S2052519213010014/GP5062SUP4.ZIP.

[26] I.J. Bruno, J.C. Cole, M. Kessler, J. Luo, W.D.S. Momerwell, L.H. Purkis, B.R. Smith, R. Taylor, R.I. Cooper, S.E. Harris, A.G. Orpen, Retrieval of crystallographically-derived molecular geometry information, J. Chem. Inf. Comput. Sci. 44 (2004) 2133–2144, https://doi.org/10.1021/CI049780B.

[27] S.J. Cottrell, T.S.G. Olsson, R. Taylor, J.C. Cole, J.W. Liebeschuetz, Validating and understanding ring conformations using small molecule crystallographic data, J. Chem. Inf. Model. 52 (2012) 956–962, https://doi.org/10.1021/CI200439D.

[28] M.A. Spackman, D. Jayatilaka, Hirshfeld surface analysis, CrystEngComm 11 (2009) 19–32, https://doi.org/10.1039/B818330A.

[29] S. Rossi, E. Gazzola, P. Capaldo, G. Borile, F. Romanato, Grating-coupled surface plasmon resonance (GC-SPR) optimization for phase-interrogation biosensing in a microfluidic chamber, Sensors 18 (2018) 1621, https://doi.org/10.3390/S18051621.

[30] H.V. Ribeiro Filho, J.V. Guerra, R. Cagliari, F.A.H. Batista, A. Le Maire, P.S. L. Oliveira, A.C.M. Figueira, Exploring the mechanism of PPARγ phosphorylation mediated by CDK5, J. Struct. Biol. 207 (2019) 317–326, https://doi.org/10.1016/J.JSB.2019.07.007.

[31] Z.K. Bagewadi, T.M. Yunus Khan, B. Gangadharappa, A. Kamalapurkar, S. Mohamed Shamsudeen, D.A. Yaraguppi, Molecular dynamics and simulation analysis against superoxide dismutase (SOD) target of Micrococcus luteus with secondary metabolites from Bacillus licheniformis recognized by genome mining approach, Saudi J. Biol. Sci. 30 (2023) 103753, https://doi.org/10.1016/J.SJBS.2023.103753.

[32] G. Cazzaniga, A. Tresoldi, A. Gelain, F. Meneghetti, M. Mori, S. Villa, Eco-friendly bio-based solvents for the acetylation of the amino group of amino acids, Chem. Biodivers. 21 (2024) e202301729, https://doi.org/10.1002/CBDV.202301729.

[33] M.F. Terra, M. García-Arévalo, T.M. Avelino, K.Y. Degaki, C.C. Malospirito, M. de Carvalho, F.R. Torres, Â. Saito, A.C.M. Figueira, AM-879, a PPARy non-agonist and Ser273 phosphorylation blocker, promotes insulin sensitivity without adverse

effects in mice, Metabol Open 17 (2023) 100221, https://doi.org/10.1016/J.METOP.2022.100221.
[34] G. Tomasello, I. Armenia, G. Molla, The protein imager: a full-featured online molecular viewer interface with server-side HQ-rendering capabilities, Bioinformatics 36 (2020) 2909–2911, https://doi.org/10.1093/BIOINFORMATICS/BTAA009.
[35] A.C. Wallace, R.A. Laskowski, J.M. Thornton, LIGPLOT: a program to generate schematic diagrams of protein-ligand interactions, Protein Eng. Des. Sel. 8 (1995) 127–134, https://doi.org/10.1093/PROTEIN/8.2.127.
[36] M.C. Burla, R. Caliandro, B. Carrozzini, G.L. Cascarano, C. Cuocci, C. Giacovazzo, M. Mallamo, A. Mazzone, G. Polidori, Crystal structure determination and refinement via SIR2014, J. Appl. Crystallogr. 48 (2015) 306–309, https://doi.org/10.1107/S1600576715001132.
[37] G.M. Sheldrick, Crystal structure refinement with SHELXL, Acta Crystallogr C Struct Chem 71 (2015) 3–8, https://doi.org/10.1107/S2053229614024218.
[38] L.J. Farrugia, WinGX and ORTEP for windows: an update, J. Appl. Crystallogr. 45 (2012) 849–854, https://doi.org/10.1107/S0021889812029111.
[39] M. Nardelli, PARST95 – an update to PARST: a system of Fortran routines for calculating molecular structure parameters from the results of crystal structure analyses, J. Appl. Crystallogr. 28 (1995), https://doi.org/10.1107/S0021889895007138, 659–659.
[40] C.F. MacRae, I. Sovago, S.J. Cottrell, P.T.A. Galek, P. McCabe, E. Pidcock, M. Platings, G.P. Shields, J.S. Stevens, M. Towler, P.A. Wood, Mercury 4.0: from visualization to analysis, design and prediction, J. Appl. Crystallogr. 53 (2020) 226–235, https://doi.org/10.1107/S1600576719014092.
[41] P.R. Spackman, M.J. Turner, J.J. McKinnon, S.K. Wolff, D.J. Grimwood, D. Jayatilaka, M.A. Spackman, CrystalExplorer: a program for Hirshfeld surface analysis, visualization and quantitative analysis of molecular crystals, J. Appl. Crystallogr. 54 (2021) 1006–1011, https://doi.org/10.1107/S1600576721002910.
[42] R.A. Friesner, J.L. Banks, R.B. Murphy, T.A. Halgren, J.J. Klicic, D.T. Mainz, M. P. Repasky, E.H. Knoll, M. Shelley, J.K. Perry, D.E. Shaw, P. Francis, P.S. Shenkin, Glide: a new approach for rapid, accurate docking and scoring. 1. Method and assessment of docking accuracy, J. Med. Chem. 47 (2004) 1739–1749, https://doi.org/10.1021/JM0306430.
[43] W.L. Jorgensen, J. Chandrasekhar, J.D. Madura, R.W. Impey, M.L. Klein, Comparison of simple potential functions for simulating liquid water, J. Chem. Phys. 79 (1983) 926–935, https://doi.org/10.1063/1.445869.
[44] R.J. Loncharich, B.R. Brooks, R.W. Pastor, Langevin dynamics of peptides: the frictional dependence of isomerization rates of N-acetylalanyl-N′-methylamide, Biopolymers 32 (1992) 523–535, https://doi.org/10.1002/BIP.360320508.
[45] J. Åqvist, P. Wennerström, M. Nervall, S. Bjelic, B.O. Brandsdal, Molecular dynamics simulations of water and biomolecules with a Monte Carlo constant pressure algorithm, Chem. Phys. Lett. 384 (2004) 288–294, https://doi.org/10.1016/J.CPLETT.2003.12.039.
[46] S. Genheden, U. Ryde, The MM/PBSA and MM/GBSA methods to estimate ligand-binding affinities, Expet Opin. Drug Discov. 10 (2015) 449–461, https://doi.org/10.1517/17460441.2015.1032936.
[47] D. Capelli, C. Cerchia, R. Montanari, F. Loiodice, P. Tortorella, A. Laghezza, L. Cervoni, G. Pochetti, A. Lavecchia, Structural basis for PPAR partial or full activation revealed by a novel ligand binding mode, Sci. Rep. 6 (2016) 1–12, https://doi.org/10.1038/srep34792.
[48] C. Vonrhein, C. Flensburg, P. Keller, A. Sharff, O. Smart, W. Paciorek, T. Womack, G. Bricogne, Data processing and analysis with the autoPROC toolbox, Acta Crystallogr D Biol Crystallogr 67 (2011) 293–302, https://doi.org/10.1107/S0907444911007773.
[49] J. Navaza, AMoRe: an automated package for molecular replacement, Acta Crystallogr. A 50 (1994) 157–163, https://doi.org/10.1107/S0108767393007597.
[50] A.T. Brünger, P.D. Adams, G.M. Clore, W.L. Delano, P. Gros, R.W. Grossekunstleve, J.S. Jiang, J. Kuszewski, M. Nilges, N.S. Pannu, R.J. Read, L.M. Rice, T. Simonson, G.L. Warren, Crystallography & NMR system: a new software suite for macromolecular structure determination, Acta Crystallogr D Biol Crystallogr 54 (1998) 905–921, https://doi.org/10.1107/S0907444998003254.
[51] A.T. Brunger, Version 1.2 of the crystallography and NMR system, Nat. Protoc. 2 (2007) 2728–2733, https://doi.org/10.1038/nprot.2007.406.
[52] R. Torices, A.J. Muñoz-Pajares, PHENIX: an R package to estimate a size-controlled phenotypic integration index, Appl. Plant Sci. 3 (2015) 1400104, https://doi.org/10.3732/APPS.1400104.